

1 **Post-Transcriptional Regulation of Antiviral Gene Expression by N6-Methyladenosine**

2

3 Michael J. McFadden ¹, Alexa B.R. McIntyre ^{2,3,a*}, Haralambos Mourelatos ^{4*}, Nathan S. Abell
4 ^{5,6*}, Nandan S. Gokhale ^{1,b}, H el ene Ipas ⁵, Blerta Xhemal e ^{5**}, Christopher E. Mason ^{2,3,7**},
5 Stacy M. Horner^{† 1,8}

6

7 Affiliations:

8 ¹ Department of Molecular Genetics and Microbiology, Duke University Medical Center,
9 Durham, NC 27710, USA.

10 Michael J. McFadden; michael.mcfadden@duke.edu, Nandan S. Gokhale;
11 ngokhale@uw.edu, Stacy M. Horner; stacy.horner@duke.edu

12 ² Department of Physiology and Biophysics, Weill Cornell Medicine, New York, NY 10021,
13 USA.

14 Alexa B.R. McIntyre; abm237@cornell.edu, Christopher E. Mason;
15 chm2042@med.cornell.edu

16 ³ Tri-Institutional Program in Computational Biology and Medicine, New York City, NY
17 10021, USA.

18 Alexa B.R. McIntyre; abm237@cornell.edu, Christopher E. Mason;
19 chm2042@med.cornell.edu

20 ⁴ Weill Cornell/Rockefeller/Memorial Sloan Kettering Tri-Institutional MD-PhD Program,
21 New York, NY, 10021, USA.

22 Haralambos Mourelatos; ham4006@med.cornell.edu

23 ⁵ Department of Molecular Biosciences, University of Texas at Austin, Austin, TX 78712,
24 USA.

25 Nathan S. Abell; nsabell@stanford.edu, H el ene Ipas; helene.ipas@utexas.edu, Blerta
26 Xhemal e; b.xhemalce@austin.utexas.edu.

27 ⁶ Department of Genetics, Stanford University School of Medicine, 300 Pasteur Drive,
28 Stanford, CA 94305-5324, USA.

29 Nathan S. Abell; nsabell@stanford.edu

30 ⁷ The HRH Prince Alwaleed Bin Talal Bin Abdulaziz Alsaud Institute for
31 Computational Biomedicine, Weill Cornell Medicine, New York, NY, 10021, USA.

32 Christopher E. Mason; chm2042@med.cornell.edu

33 ⁸ Department of Medicine, Duke University Medical Center, Durham, NC 27710, USA.

34 Stacy M. Horner; stacy.horner@duke.edu

35

36 Current address:

37 ^a Department of Molecular Life Sciences, University of Zurich, Switzerland

38 ^b Department of Immunology, University of Washington, Seattle WA 98109

39

40 *, ** Equal Contribution

41

42 † Corresponding author

43 Correspondence to Stacy M. Horner (stacy.horner@duke.edu)

44

45

46 **Summary**

47 Type I interferons (IFN) induce hundreds of IFN-stimulated genes (ISGs) in response to
48 viral infection. These ISGs require strict regulation for an efficient and controlled antiviral
49 response, but post-transcriptional controls of these genes have not been well defined. Here, we
50 identify a new role for the RNA base modification *N*6-methyladenosine (m⁶A) in the regulation of
51 ISGs. Using ribosome profiling and quantitative mass spectrometry, coupled with m⁶A-
52 immunoprecipitation and sequencing, we identified a subset of ISGs, including *IFITM1*, whose
53 translation is enhanced by m⁶A and the m⁶A methyltransferase proteins METTL3 and METTL14.
54 We further determined that the m⁶A reader YTHDF1 increases the expression of *IFITM1* in an
55 m⁶A binding-dependent manner. Importantly, we found that the m⁶A methyltransferase complex
56 promotes the antiviral activity of type I IFN. Thus, these studies identify m⁶A as a post-
57 transcriptional control of ISG translation during the type I IFN response for antiviral restriction.

58

59 **Introduction**

60 The IFN family cytokines are potent inhibitors of viral infection that induce hundreds of
61 ISGs, many of which have antiviral activity (Gonzalez-Navajas et al., 2012; Schoggins and Rice,
62 2011). Type I IFNs (IFN- α and IFN- β) are produced in response to viral infection, and they activate
63 autocrine and paracrine signaling responses through the JAK-STAT pathway (Stark and Darnell,
64 2012). Specifically, type I IFNs bind to a dimeric receptor (IFNAR), composed of two subunits,
65 IFNAR1 and IFNAR2. IFNAR engagement then activates the Janus kinases JAK1 and TYK2,
66 which phosphorylate the transcription factors STAT1 and STAT2, inducing their hetero-
67 dimerization and interaction with IRF9, to form the ISGF3 transcription factor complex. ISGF3
68 then translocates into the nucleus, where it binds to IFN-stimulated response elements within the
69 promoters of ISGs to elicit their transcriptional activation (Stark and Darnell, 2012). Many of these
70 ISGs encode antiviral effector proteins that inhibit multiple stages of viral replication and thus
71 establish an early defense against viral replication (Schoggins, 2019). Dysregulation of type I IFNs
72 can lead to viral susceptibility or autoimmune disease (Banchereau and Pascual, 2006; Teijaro,
73 2016), demonstrating the importance of tight regulatory control of both IFN activation and the IFN
74 response. Indeed, both activation and suppression of the type I IFN response are coordinated at
75 multiple levels, such as by epigenetic modifiers (Fang et al., 2012; Huang et al., 2002; Liu et al.,
76 2002) or by post-transcriptional mechanisms including microRNA regulation and alternative
77 splicing (Forster et al., 2015; West et al., 2019). However, our overall understanding of post-
78 transcriptional regulation of ISG expression is still emerging. Additionally, while a number of
79 studies have identified subsets of ISGs that have unique transcriptional regulators, other

80 mechanisms that govern the regulation of subclasses of ISGs have not been well characterized
81 (Froggatt et al., 2019; Perwitasari et al., 2011; Seifert et al., 2019).

82 The RNA base modification m⁶A is deposited on RNA by a methyltransferase complex of
83 METTL3 and METTL14 (METTL3/14), among other proteins (Liu et al., 2014). m⁶A coordinates
84 biological processes through various effects on modified mRNAs (Meyer and Jaffrey, 2017; Shi
85 et al., 2019), including increased mRNA turnover and translation, as well as other processes.
86 These effects are mediated by m⁶A reader proteins, such as YTHDF proteins (Liu et al., 2019a;
87 Wang et al., 2014; Wang et al., 2015). Specifically, YTHDF1 increases translation (Wang et al.,
88 2015), YTHDF2 mediates mRNA degradation (Wang et al., 2014), and YTHDF3 cooperatively
89 enhances both of these processes (Shi et al., 2017), although in some cases these proteins may
90 have overlapping functions (Zaccara and Jaffrey, 2020). Through the actions of m⁶A reader
91 proteins, m⁶A can regulate infection by many viruses through modulation of both viral and host
92 transcripts (Williams et al., 2019). We recently profiled changes to the m⁶A landscape of host
93 mRNAs during *Flaviviridae* infection and identified both proviral and antiviral transcripts regulated
94 by m⁶A during infection (Gokhale et al., 2019). Others have found that m⁶A prevents RNA sensing
95 or regulates the expression of signaling molecules involved in the production of cytokines such
96 as type I IFNs (Chen et al., 2019; Durbin et al., 2016; Feng et al., 2018; Kariko et al., 2005; Lu et
97 al., 2020; Zheng et al., 2017) and that m⁶A can destabilize the *IFNB1* transcript, thereby directly
98 regulating the production of IFN- β (Rubio et al., 2018; Winkler et al., 2019). Therefore, m⁶A plays
99 important roles in viral infection and the antiviral response (Zhang et al., 2019a); however, a role
100 for m⁶A in the response to type I IFN and the production of ISGs has not been described.

101 Here, we mapped m⁶A in the IFN- β -induced transcriptome and identified many ISGs that
102 are m⁶A-modified. We found that METTL3/14 and m⁶A promote the translation of certain m⁶A-
103 modified ISGs, in part through interactions between the transcripts of m⁶A-modified ISGs and the
104 m⁶A reader protein YTHDF1. Importantly, we found that METTL3/14 and m⁶A-mediated
105 enhancement of ISG expression promotes the antiviral effects of the IFN response, as
106 METTL3/14 perturbation affected the replication of vesicular stomatitis virus (VSV) in IFN- β -
107 primed cells. Together, these results establish m⁶A as a post-transcriptional regulator of ISGs for
108 an effective cellular antiviral response.

109

110 **Results**

111 **METTL3/14 regulates the translation of certain ISGs.**

112 IFN- β induces the transcription of ISGs to shape the innate response to viral infection
113 (Schoggins and Rice, 2011). To investigate whether m⁶A regulates the type I IFN response, we

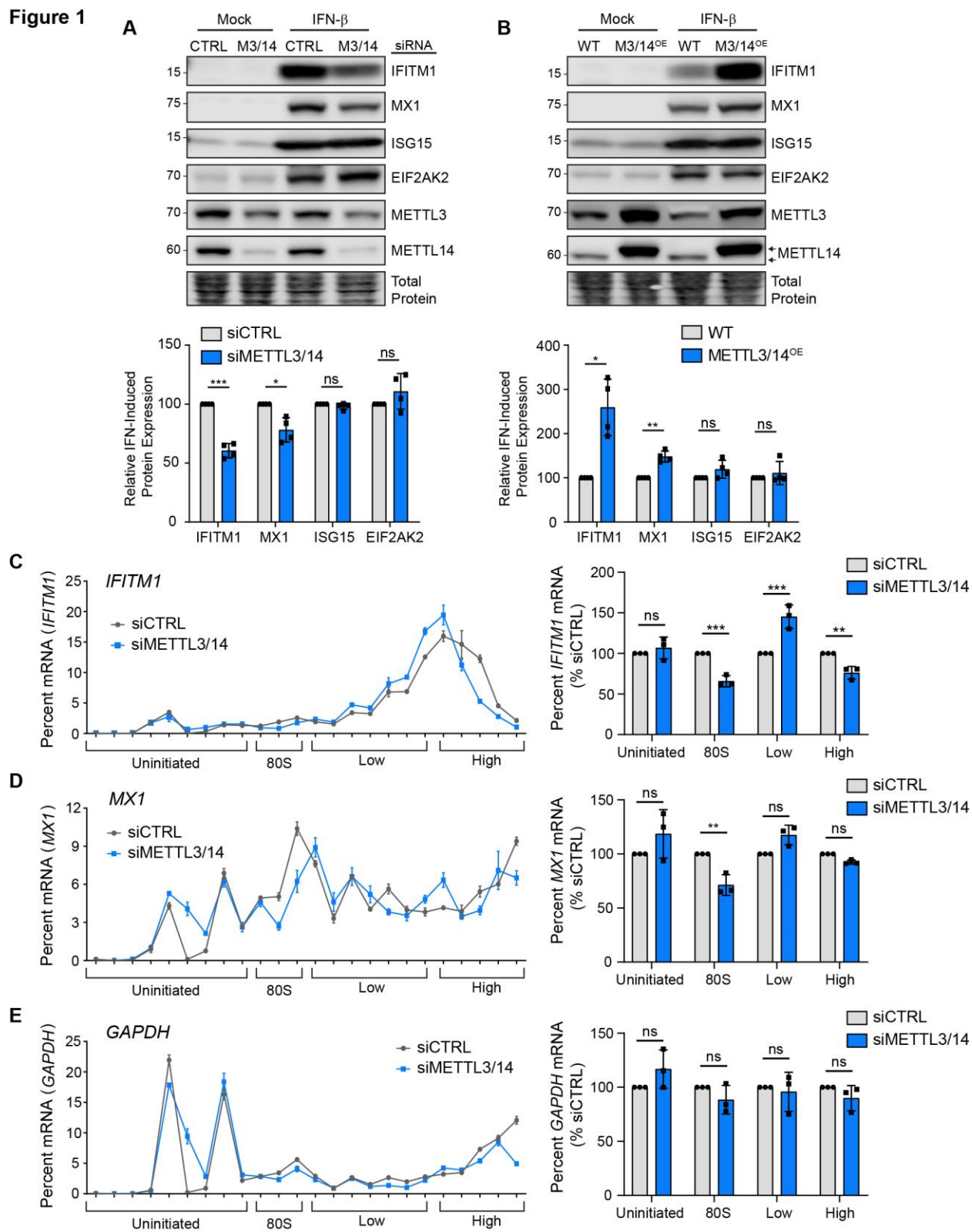
114 measured the IFN- β -induced expression of several ISGs with known antiviral functions
115 (Schoggins, 2014) following depletion of the m⁶A methyltransferase complex METTL3/14 in Huh7
116 cells. The IFN- β -induced protein expression of the ISGs IFITM1 and MX1, but not ISG15 and
117 EIF2AK2 (also called PKR), was reduced following depletion of METTL3/14 (Figure 1A; see
118 Methods for information on IFITM1 antibody specificity). Similar results were also seen following
119 METTL3/14 depletion in A549 cells, primary neonatal human dermal fibroblasts (NHDF), and also
120 at multiple time points (8 h, 16 h, and 24 h) after IFN- β in Huh7 cells (Figure S1A-1C); however
121 we note MX1 protein levels were not as strongly affected in A549 and NHDF cells as in Huh7
122 cells. Conversely, overexpression of METTL3/14 increased the abundance of IFITM1 and MX1,
123 but not ISG15 and EIF2AK2, in response to IFN- β in Huh7 cells (Figure 1B). Importantly, the
124 METTL3/14-regulated ISGs, IFITM1 and MX1, were not expressed without stimulation of cells by
125 IFN- β (Figure 1A-1B). Therefore, any confounding effects of METTL3/14 perturbation on
126 endogenous IFN- β production are negligible for these experiments.

127 The METTL3/14 m⁶A methyltransferase complex regulates many aspects of mRNA
128 metabolism (Liu et al., 2019a). To determine how METTL3/14 regulates the protein abundance
129 of certain ISGs, we first tested whether METTL3/14 depletion led to a decrease in induction of
130 ISG mRNA in response to IFN- β . We measured the induction of ISG mRNA in response to IFN- β
131 over a timecourse using RT-qPCR (Figure S1D). Neither the mRNA abundance nor the kinetics
132 of IFN- β -mediated induction of the METTL3/14-regulated ISGs *IFITM1* and *MX1* were affected by
133 METTL3/14 depletion. The mRNA levels of the non-METTL3/14-regulated ISG *EIF2AK2* was
134 unaffected, while *ISG15* mRNA was increased (Figure S1D). These data indicate that the mRNA
135 abundance of *IFITM1* and *MX1* does not underlie the observed differences in protein levels,
136 suggesting that neither the transcription nor the mRNA stability of these ISGs are regulated by
137 METTL3/14 (Figure S1D). Further, using RNA-seq following IFN- β treatment, we noted little effect
138 of METTL3/14 depletion on the mRNA abundance of a defined set of core ISGs (Shaw et al.,
139 2017) (Figure S1E) or expressed ISGs more broadly (Table S1). These data are in agreement
140 with a previous report that found that collective ISG RNA stability is unaffected by METTL3
141 depletion (Winkler et al., 2019).

142 As both METTL3/14 and m⁶A have been shown to promote the nuclear export of certain
143 mRNAs (Lesbirel and Wilson, 2019), we also tested whether the nuclear export of select ISGs
144 was altered by METTL3/14 depletion. However, after IFN stimulation, METTL3/14 depletion did
145 not alter the nuclear-cytoplasmic ratio of the METTL3/14-regulated ISGs *IFITM1* and *MX1*, the
146 non-regulated ISGs *ISG15* and *EIF2AK2*, a non-methylated control *HPRT1* (Wang et al., 2014),

147 or the nuclear-localized control *MALAT1* (Figure S2C). Therefore, METTL3/14 does not regulate
 148 these ISGs through changes to their protein stability or nuclear export.

Figure 1



149

150 **Figure 1: METTL3/14 regulates translation of certain ISGs. (A, B)** Immunoblot analysis of
151 extracts from Huh7 cells transfected with siRNAs to METTL3/14 (M3/14) or control (CTRL) **(A)** or
152 stably overexpressing FLAG-METTL14 (M3/14^{OE}; top arrow denotes FLAG-METTL14; bottom
153 arrow denotes endogenous METTL14) **(B)** prior to mock or IFN- β (24 h) treatment. Relative ISG
154 expression from 4 replicates of (A) and (B) is quantified below relative to siCTRL +IFN- β (A) or
155 WT +IFN- β (B). **(C-E)** RT-qPCR analysis of the relative percentage of *IFITM1* (C), *MX1* (D), and
156 *GAPDH* (E) mRNA across 24 sucrose gradient fractions isolated from extracts of IFN- β -treated
157 (6 h) Huh7 cells treated with CTRL or METTL3/14 siRNA. The uninitiated (free, 40S, and 60S
158 subunits), initiated (80S), low or high molecular weight polysomes, are noted. Graphs on the right
159 show the percentages of mRNAs in combined fractions for *IFITM1*, *MX1*, or *GAPDH*. Percentages
160 from fractions were added to yield the total percentage in each category. Values are the mean \pm
161 SEM of 4 biological replicates (A-B), the mean \pm SD of 3 technical replicates, representative of 3
162 experiments (C-E, left graphs), and the mean \pm SEM of 3 biological replicates (C-E, right graphs).
163 * $p < 0.05$, ** $p < 0.01$, *** $p < 0.005$ by unpaired Student's t test (A-B), and 2-way ANOVA with
164 Sidak's multiple comparisons test (C-E). ns = not significant. See also Figure S1-S2.

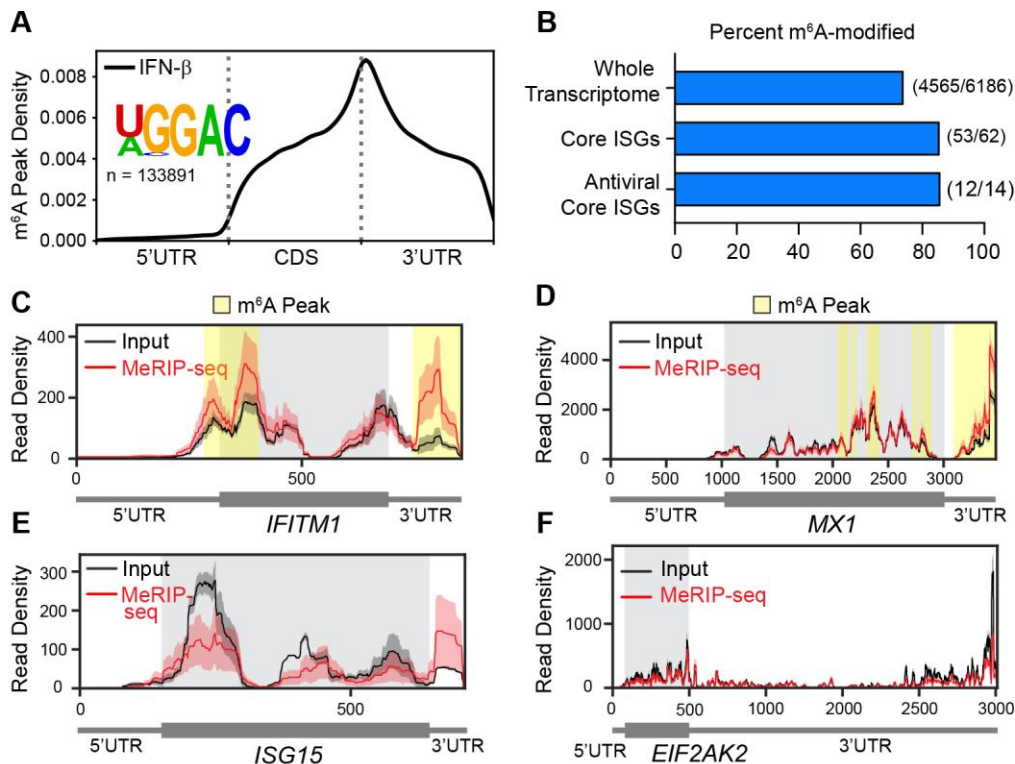
165
166 To test whether METTL3/14 regulates the translation of *IFITM1*, we measured the
167 polysome occupancy of *IFITM1* induced by IFN- β in control cells or in those depleted of
168 METTL3/14. METTL3/14 depletion did not change overall polysome density, as observed by the
169 similar relative absorption across fractions (Figure S2D). However, METTL3/14 depletion did
170 result in lower levels of *IFITM1* mRNA in the 80S fractions and a shift from the heavy to the light
171 polysome fractions (Figure 1C), indicating impaired translation of *IFITM1* following METTL3/14
172 depletion. A similar, yet less pronounced shift was observed for *MX1* (Figure 1D), while the
173 polysome occupancy of the housekeeping control gene *GAPDH* was unaffected (Figure 1E).
174 These results indicate that METTL3/14 regulates the translation of certain ISGs, such as *IFITM1*
175 and *MX1*.

176
177 **METTL3/14-regulated ISGs are modified by m⁶A.**

178 To determine whether the METTL3/14-regulated ISGs *IFITM1* and *MX1*, as well as other
179 ISGs, are m⁶A-modified, we mapped m⁶A in the IFN-induced transcriptome in Huh7 cells using
180 methylated RNA immunoprecipitation and sequencing (MeRIP-seq) (Dominissini et al., 2012;
181 Meyer et al., 2012). After defining the ISGs in this experiment (Figure S3A; Table S2), we then
182 called peaks in read coverage post-m⁶A immunoprecipitation compared to input using the MeTDiff
183 m⁶A peak caller (Cui et al., 2018) (Table S2). We observed that peaks across mRNAs were
184 enriched around the end of the coding sequence and the beginning of the 3' UTR, as expected
185 (Dominissini et al., 2012; Meyer et al., 2012) (Figure 2A). The most highly enriched RNA sequence
186 motif within peaks was [U/A]GGAC, which matches the known m⁶A motif of DRAMC (Dominissini

187 et al., 2012; Meyer et al., 2012) (Figure 2A). We found that approximately 85% percent of ISGs,
188 classified as those upregulated more than 4-fold following IFN treatment, were m⁶A-modified, as
189 compared to 74% percent of the expressed transcriptome of Huh7 cells (mean coverage ≥ 10)
190 (Figure 2B). This was consistent with a previous study that found that ISGs were m⁶A-modified at
191 a similar percentage to the transcriptome (Winkler et al., 2019). The percent of ISGs that are m⁶A-
192 modified was similar among other classes of ISGs, including a 'core' class of ISGs that are
193 evolutionarily conserved among vertebrate species and a subset of 14 of these core ISGs with
194 known antiviral functions (Shaw et al., 2017) (Figure 2B). Plotting the MeRIP-seq reads relative
195 to the input reads of individual genes can be informative of m⁶A status, as m⁶A peak calling
196 methods have known limitations (McIntyre et al., 2020). Thus, we generated plots for *IFITM1*,
197 *MX1*, *ISG15*, and *EIF2AK2* and used the m⁶A peak callers MeTDiff (Cui et al., 2018) and
198 meRIPPer (<https://sourceforge.net/projects/meripper/>) (Table S2) to reveal that the METTL3/14-
199 regulated genes *IFITM1* and *MX1* had m⁶A peaks (Figure 2C-D), while *ISG15* and *EIF2AK2*
200 lacked called m⁶A peaks (Figure 2E-F). These plots suggested that the 3' UTR of *ISG15* may also
201 contain an m⁶A site (Figure 2E). We then compared the m⁶A status of ISGs from our MeRIP-seq
202 experiment to data from previously published studies that profiled m⁶A after IFN-inducing
203 treatments, such as dsDNA (Rubio et al., 2018) or human cytomegalovirus (HCMV) infection
204 (Winkler et al., 2019) (Figure S3B). This comparison showed consistent prediction of m⁶A
205 methylation status for core antiviral ISGs among all three studies (Figure S3B). Indeed, dsDNA
206 treatment potently activates IFN production and elicited m⁶A modification of the same core
207 antiviral ISGs found in our experiment. Infection with HCMV also elicited m⁶A modification of
208 certain ISGs, although fewer peaks were called in these ISGs after HCMV infection than after
209 IFN- β treatment or dsDNA treatment (Figure S3B). We note this virus encodes factors to dampen
210 IFN signaling (Miller et al., 1999), therefore ISGs are likely not as strongly induced as compared
211 to dsDNA or IFN- β treatment. The presence of m⁶A on many ISGs suggests that m⁶A may
212 regulate the antiviral type I IFN response.

Figure 2



213

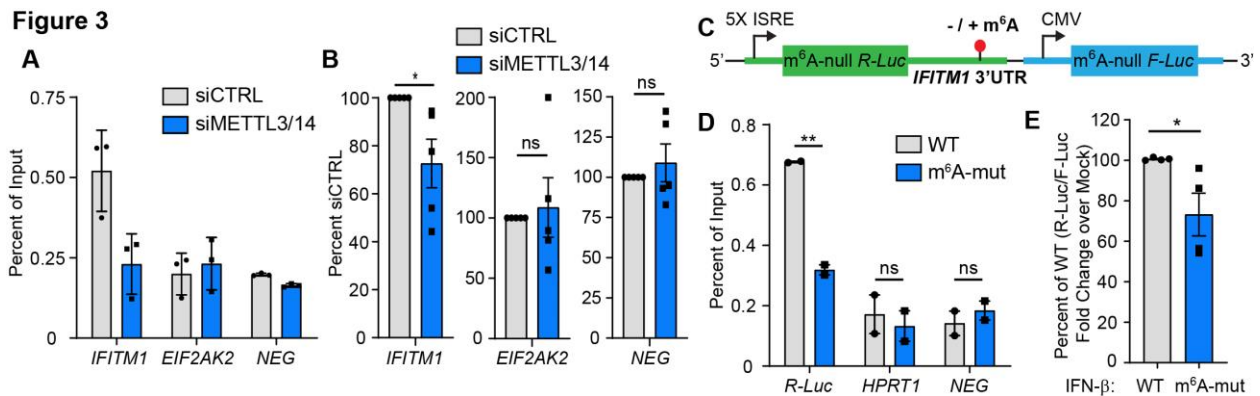
214 **Figure 2: METTL3/14-regulated ISGs are modified by m⁶A.** (A) Metagenome plot of predicted m⁶A
215 distribution across the transcriptome following IFN- β treatment (8 h), with relative positions of
216 DRACH motif sites under statistically significant peaks plotted, as well as the most highly enriched
217 motif under peaks. (B) The percent of genes modified by m⁶A in the expressed transcriptome,
218 genes with mRNA induction \geq 4-fold in response to IFN- β treatment (ISGs), a group of core ISGs
219 conserved in vertebrate species (Shaw et al., 2017), or a subset of these core ISGs with antiviral
220 functions (Shaw et al., 2017). (C-F) Read coverage plots of MeRIP (red) and input (black) reads
221 in *IFITM1* (C), *MX1* (D), *ISG15* (E), and *EIF2AK2* (F) transcripts. Variance between biological
222 replicates is represented by red and black shading around read coverage. Gray shading
223 represents coding sequence, yellow shading represents m⁶A peaks called by MeTDiff (Cui et al.,
224 2018) and meRIPPer (<https://sourceforge.net/projects/meripper/>)
225 software. All analyses are performed on 3 biological replicates. See also Figure S3.

226

227 m⁶A modification in the 3' UTR of *IFITM1* enhances its translation.

228 m⁶A is known to enhance the translation of certain mRNAs (Coots et al., 2017; Gokhale
229 et al., 2019; Lin et al., 2016; Mao et al., 2019; Wang et al., 2015). Specifically, the m⁶A reader
230 protein YTHDF1 can recognize m⁶A within 3' UTRs and associate with eukaryotic translation
231 initiation factors such as eIF3 to enhance the translation of m⁶A-modified transcripts (Wang et al.,
232 2015). To determine whether the translational regulation of ISGs by METTL3/14 is elicited through
233 m⁶A, we used *IFITM1* as a model METTL3/14-regulated ISG. We first determined the effect of

234 METTL3/14 depletion on m⁶A modification of *IFITM1*. MeRIP-RT-qPCR revealed that *IFITM1*
235 mRNA was enriched above the m⁶A-negative ISG *EIF2AK2* and a spiked-in m⁶A-negative
236 synthetic RNA, confirming that it contains m⁶A. METTL3/14 depletion reduced the m⁶A-
237 enrichment of *IFITM1* mRNA but not of the m⁶A-negative *EIF2AK2* transcript or the m⁶A-negative
238 synthetic RNA (Figure 3A-B). These data reveal that *IFITM1* is m⁶A-modified by METTL3/14.
239



240

241 **Figure 3: m⁶A modification of the *IFITM1* 3' UTR enhances translation.** (A) Representative
242 MeRIP-RT-qPCR analysis of relative m⁶A level of ISGs induced by IFN-β (8 h) in Huh7 cells
243 treated with non-targeting control (siCTRL) or METTL3/14 siRNA and spiked-in m⁶A-negative
244 (NEG) oligonucleotides. (B) Relative percent enrichment of each gene in (A), normalized to
245 siCTRL, from 5 biological replicates. (C) Schematic of WT and mutant ISRE-m⁶A-null *Renilla*
246 luciferase (*R-Luc*) *IFITM1* 3' UTR reporters that also express m⁶A-null firefly luciferase (*F-Luc*)
247 from a separate promoter. (D) MeRIP-RT-qPCR analysis of relative m⁶A level of WT and m⁶A-
248 mut *IFITM1* 3' UTR reporter RNA from transfected Huh7 cells treated with IFN-β (8 h). (E) Relative
249 luciferase activity (*R-Luc*/*F-Luc*) in IFN-β induced (8 h, relative to mock) WT and m⁶A-mut *IFITM1*
250 3' UTR reporters. Values are the mean ± SD of 3 technical replicates representative of 5 biological
251 replicates (A); the mean ± SEM of 5 biological replicates (B); the mean ± SEM of 2 biological
252 replicates (D), or mean ± SEM of 4 biological replicates (E). * p < 0.05, ** p < 0.01 by unpaired
253 Student's t test. ns = not significant.

254

255 Having confirmed that *IFITM1* is m⁶A modified, we next generated a luciferase reporter
256 that contains an IFN-stimulated response element (ISRE) promoter-driven *Renilla* luciferase in
257 which all DRAC motifs were ablated (m⁶A-null *R-Luc*) (Gokhale et al., 2019) fused to the wild type
258 (WT) *IFITM1* 3' UTR, or an analogous 3' UTR sequence in which the four putative m⁶A motifs
259 under the m⁶A peak in the 3' UTR in *IFITM1* were inactivated by A→G transitions (m⁶A-mut)
260 (Figure 3C). These constructs also express a CMV promoter-driven m⁶A-null firefly luciferase
261 gene as a control. The m⁶A modification status of the *IFITM1* 3' UTR reporter was first assessed
262 using MeRIP-RT-qPCR after IFN-β treatment. The WT *IFITM1* 3' UTR reporter had increased

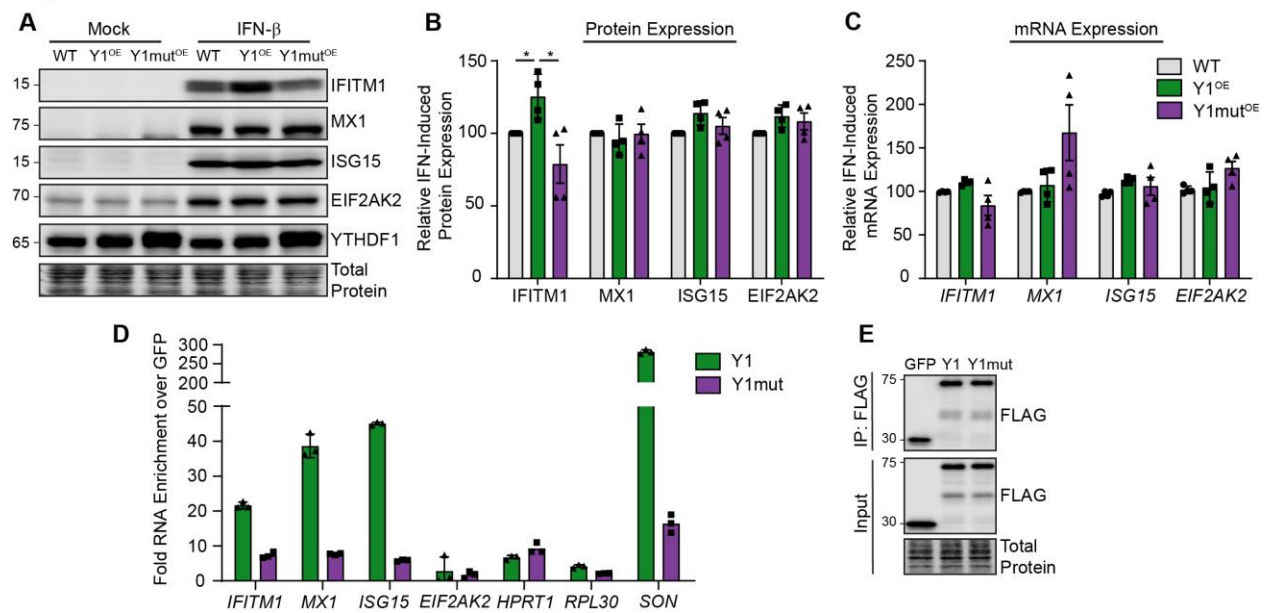
263 m⁶A modification compared to the m⁶A-mut *IFITM1* 3' UTR reporter, as well as the negative
264 controls: *HPRT1*, which does not contain m⁶A (Wang et al., 2014), and an m⁶A-negative synthetic
265 RNA control (Figure 3D). We next compared the production of the *Renilla* luciferase protein,
266 relative to firefly luciferase, from the WT and m⁶A-mut *IFITM1* 3' UTR reporters by measuring
267 luciferase activity. We found that the relative luciferase activity of the m⁶A-mut *IFITM1* 3'UTR
268 reporter was significantly decreased following IFN- β treatment compared to the WT *IFITM1* 3'
269 UTR reporter (Figure 3E). Together, these data suggest that METTL3/14 regulates *IFITM1*
270 translation through addition of m⁶A to the 3' UTR and that m⁶A within the *IFITM1* 3' UTR is
271 sufficient to enhance its translation.

272

273 **YTHDF1 enhances *IFITM1* protein expression in an m⁶A-dependent fashion.**

274 The m⁶A binding protein YTHDF1 enhances translation of a number of m⁶A-modified
275 genes (Wang et al., 2015). To test if YTHDF1 elicited the translation-promoting effects of m⁶A on
276 ISGs, we stably overexpressed YTHDF1 (Y1^{OE}) or an m⁶A binding-deficient YTHDF1 protein (Xu
277 et al., 2015) (Y1mut^{OE}) in Huh7 cells and measured the IFN-induced expression of ISGs 24 hours
278 later. Overexpression of YTHDF1 was sufficient to increase *IFITM1* protein expression in
279 response to IFN- β , while overexpression of the m⁶A binding-deficient YTHDF1 protein (Y1mut^{OE})
280 did not increase *IFITM1* abundance (Figure 4A-B). Importantly, wild-type and mutant YTHDF1
281 overexpression did not significantly affect the levels of *IFITM1* mRNA following IFN- β treatment,
282 suggesting that YTHDF1 does not directly regulate IFN signaling or *IFITM1* mRNA stability (Figure
283 4C). Neither the IFN-induced expression of the m⁶A-containing ISG *MX1*, nor the non-m⁶A
284 containing ISGs *ISG15* and *EIF2AK2*, were significantly altered by YTHDF1 overexpression
285 (Figure 4A-B). Interestingly, we found that WT YTHDF1 bound to the transcripts of *IFITM1*, *MX1*,
286 *ISG15*, and the m⁶A-positive control *SON* (Wang et al., 2014), while the m⁶A-binding-defective
287 YTHDF1 mutant protein did not. The non-m⁶A containing mRNAs *EIF2AK2* and *RPL30* (Wang et
288 al., 2015) did not bind to either protein (Figure 4D-E). Together, these results reveal that YTHDF1
289 binds to m⁶A on *IFITM1* and enhances its translation. The apparent m⁶A-dependent binding of
290 YTHDF1 to *ISG15* suggests that *ISG15* is actually m⁶A-modified. In fact, plotting MeRIP-seq
291 reads over input reads for *ISG15* did show a potential region of m⁶A enrichment in its 3' UTR
292 (Figure 2E), although this was not identified as significant by two peak callers (Table S2). Taken
293 together, these data suggest that YTHDF1 has transcript-specific roles in promoting translation,
294 as it bound *IFITM1*, *MX1*, and *ISG15*, but its overexpression was only sufficient to significantly
295 increase the protein production of *IFITM1*.

Figure 4



296

297 **Figure 4: YTHDF1 enhances IFITM1 protein expression in an m⁶A-dependent fashion. (A)**
 298 Immunoblot analysis of extracts from Huh7 cells stably overexpressing FLAG-YTHDF1 WT (Y1^{OE})
 299 or FLAG-YTHDF1 W465A (Xu et al., 2015) (Y1mut^{OE}) following mock or IFN-β (24 h) treatment.
 300 **(B)** Quantification of ISG expression following IFN-β from 3 independent experiments of (A),
 301 normalized to total protein and graphed relative to siCTRL. **(C)** RT-qPCR analysis of ISG mRNA
 302 expression normalized to HPRT1 in Huh7 cells stably overexpressing FLAG-YTHDF1 WT (Y1^{OE})
 303 or W465A (Y1mut^{OE}) after IFN-β (24 h) treatment **(D)** RT-qPCR analysis of enrichment of mRNAs
 304 following immunoprecipitation of FLAG-YTHDF1 WT (Y1) or W465A (Mut) compared to FLAG-
 305 GFP from Huh7 cells following IFN-β (8 h). IP values are normalized to input values and plotted
 306 as fold enrichment over GFP. **(E)** Immunoblot of FLAG-immunoprecipitated and input fractions
 307 used in (D). Values in (B-C) are the mean ± SEM of 3 biological replicates. * p < 0.05, by Kruskal-
 308 Wallis with Dunn's multiple comparisons test. Everything unlabeled was not significant with p >
 309 0.05. Values in (D) are the mean ± SD of 3 technical replicates and are representative of 4
 310 independent experiments.

311

312 **METTL3/14 and m⁶A promote the translation of a subset of ISGs.**

313 Having demonstrated that m⁶A supports the translation of two ISGs (*IFITM1* and *MX1*),
 314 and that m⁶A is present on many ISGs, we next sought to identify additional ISGs whose protein
 315 expression is regulated by METTL3/14. To this end, we employed quantitative mass
 316 spectrometry-based proteomics with stable isotope labeling of amino acids (SILAC) to compare
 317 the proteomes of siCTRL and siMETTL3/14 cells after IFN-β treatment (Table S3). The effect of
 318 siMETTL3/14 compared to siCTRL on protein abundance is centered at a log ratio of 0 for the
 319 majority of proteins (Figure S4A), demonstrating that METTL3/14 depletion does not have a global
 320 effect on protein levels after IFN-β treatment. We determined which proteins are ISGs by defining

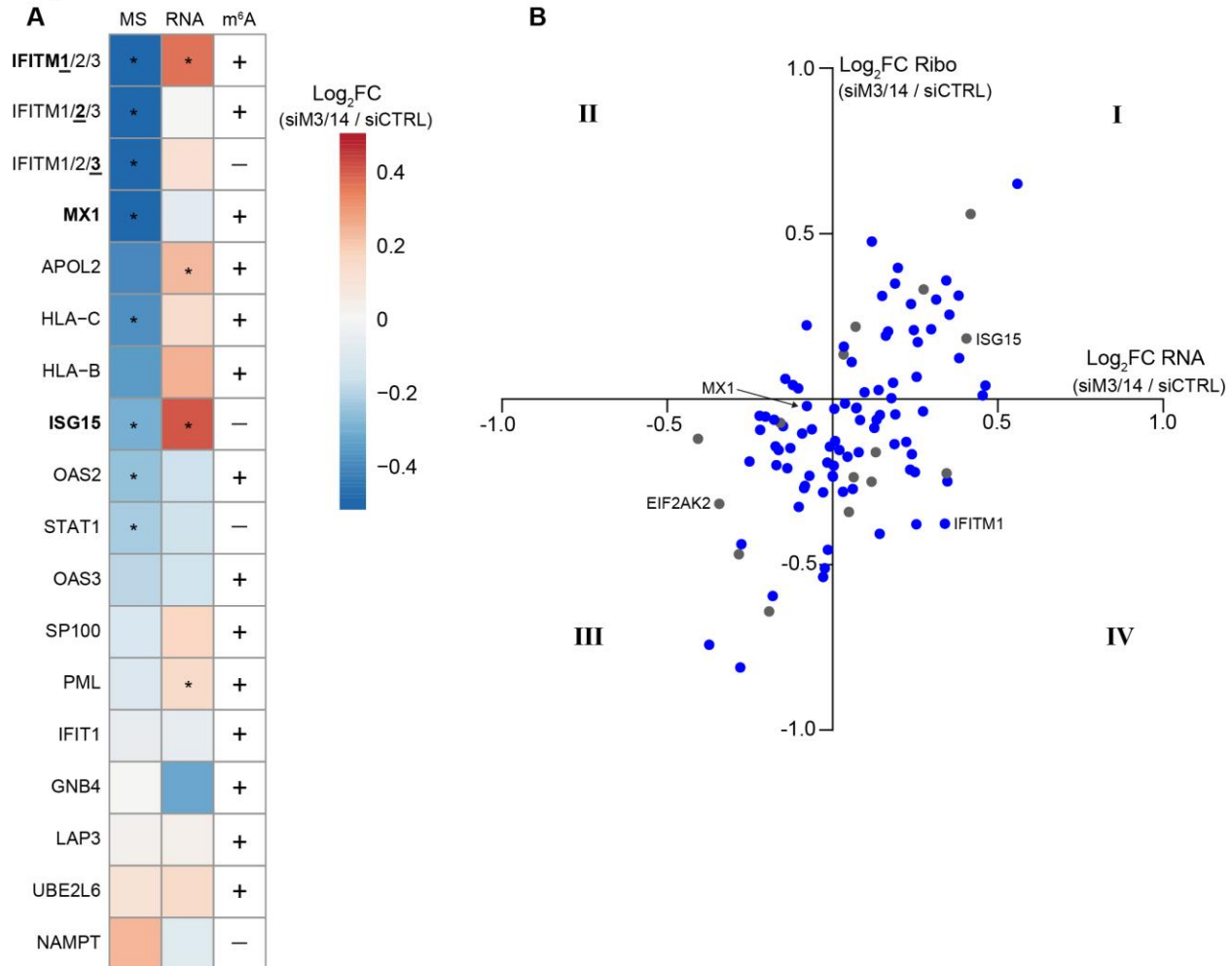
321 ISGs as genes upregulated >2-fold by IFN- β treatment in our previous RNA-seq experiment
322 (Table S1). While mass spectrometry detection of ISGs was limited (n=18), we did identify a
323 number of METTL3/14-regulated ISGs (Figure 5A, MS). The protein expression of most of these
324 ISGs was decreased following METTL3/14 depletion, and these ISGs included the previously
325 identified m⁶A-modified IFITM1 (peptides corresponding to IFITM1/2/3) and MX1, as well as
326 additional antiviral ISGs such as OAS2 and the different HLA-C chains (Figure 5A), which are
327 also m⁶A-modified. We also compared these data to our previous RNA-seq experiment (Table
328 S1) to determine whether the effects of METTL3/14 on the protein level of these ISGs is
329 determined by regulation of their mRNA expression. Importantly, following METTL3/14 depletion,
330 the ISGs in this experiment that were decreased at the protein level did not also have a decrease
331 in mRNA abundance, suggesting they may be regulated at the translation level, as our earlier
332 polysome profiling indicated for IFITM1 and MX1 (Figure 1C-D; 5A, RNA). We note that not all
333 m⁶A-modified ISGs identified by mass spectrometry were regulated by METTL3/14 depletion
334 (Figure 5A, m⁶A). This suggests that METTL3/14 and m⁶A regulate a subset of ISGs and support
335 their protein expression.

336 As a complementary approach, we also used Ribo-seq to more broadly define the role of
337 METTL3/14 in translational regulation of ISGs (Table S4). As ribosome profiling relies on digestion
338 of mRNA that is not ribosome-bound, we first confirmed that reads in the untranslated regions
339 were depleted (Figure S4B). Then we analyzed the top 100 most highly-induced ISGs (Table S1)
340 that were actively translated (base mean >25) and compared the effect of METTL3/14 depletion
341 on ribosome density (Ribo) to mRNA abundance from our previous RNA-seq analysis (RNA)
342 (Figure 5B; Figure S4C; Table S1). METTL3/14 depletion overall appeared to result in decreased
343 ribosome occupancy among many of these ISGs (66/100, including *IFITM1*), without having any
344 generalized effect on their mRNA abundance (Figure S4C). In many cases, METTL3/14 depletion
345 affected both the mRNA abundance and ribosome protection of individual ISGs similarly (Figure
346 5B, Quadrants I and III). However, for roughly a third of these genes (33/100), METTL3/14
347 depletion resulted in decreased ribosome protection, despite greater mRNA abundance (Figure
348 5B, Quadrant IV). Alternatively, very few (4/100) ISGs had both increased ribosome protection
349 and decreased mRNA abundance following METTL3/14 depletion (Figure 5B, Quadrant II). We
350 note that, of these 100 ISGs, 85 were m⁶A-modified, roughly consistent with the 74% of genes
351 that we had identified in the total expressed transcriptome as containing m⁶A (Table S2).
352 Interestingly, a number of m⁶A-modified ISGs were not regulated by METTL3/14, as measured
353 by ribosome protection or mRNA abundance, supporting a role for METTL3/14 and m⁶A in
354 regulation of only certain ISGs. These data, taken together with our quantitative mass

355 spectrometry and RNA-seq analysis, suggest that METTL3/14 regulates the translation of a
 356 subset of ISGs to support their protein expression during the type I IFN response.

357

Figure 5



358

359

360 **Figure 5: METTL3/14 regulates the translation of a subset of ISGs.** (A) 3-column heatmap
 361 shows the effect of METTL3/14 depletion on the expression of ISGs in Huh7 cells following IFN-
 362 β treatment. The first column shows the log₂ fold change of protein estimates from quantitative
 363 mass spectrometry (siMETTL3/14 over siCTRL + IFN-β 24 h; n=2 biological replicates). The
 364 second column shows log₂ fold change of mRNA reads from an independent RNA-seq
 365 experiment (siMETTL3/14 over siCTRL + IFN-β 8 h; n=3 biological replicates), and the third
 366 column indicates m⁶A status (+ indicates m⁶A-positive; - indicates m⁶A-negative) from MeRIP-
 367 seq (+ IFN-β 8 h; n=3 biological replicates). Genes include any ISGs induced more than 2-fold
 368 by IFN from RNA-seq that were also detected by mass spectrometry. ISGs investigated in other
 369 figures are shown in bold. Because IFITM1/2/3 are similar, we used this notation to indicate
 370 peptides detected from this family of proteins; however, RNA-seq fold change and m⁶A status
 371 correspond to the underlined number. * adjusted P < 0.05. (B) Four-quadrant scatterplot

372 showing the effect of METTL3/14 on the expression of ISGs. The y-axis is the log₂ fold change
373 of ribosome protected fragments from Ribo-seq (siMETTL3/14 over siCTRL), and the x-axis is
374 the log₂ fold change of mRNA reads from an independent RNA-seq experiment (siMETTL3/14
375 over siCTRL). m⁶A-modified (blue) or m⁶A-negative (gray) genes are noted. ISGs investigated in
376 other figures are labeled. See also Figure S4.

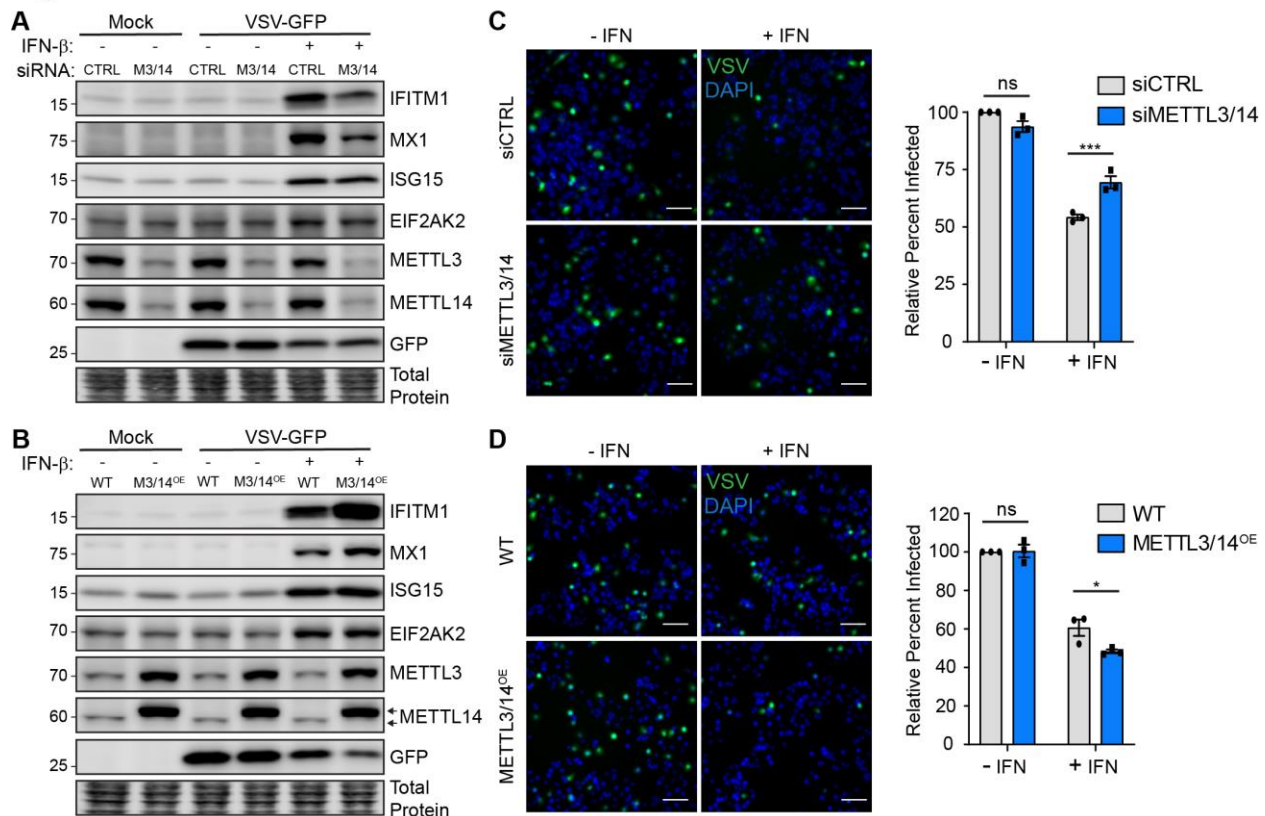
377

378 **METTL3/14 augments the antiviral effects of the IFN response.**

379 The fact that METTL3/14 enhances the expression of a subset of ISGs during the type I
380 IFN response suggests that METTL3/14 could be required for an optimal antiviral response. To
381 determine whether METTL3/14 contributes to viral restriction by type I IFN, we measured the
382 ability of type I IFN to restrict infection by the negative-sense stranded RNA virus, vesicular
383 stomatitis virus (VSV), following METTL3/14 perturbation. The VSV genome contains the m⁶A_m
384 cap modification, but as the deposition of this modification is not controlled by METTL3/14
385 (Boulias et al., 2019; Ogino and Banerjee, 2011; Sendinc et al., 2019), we would not expect VSV
386 replication to be directly affected by changes in the levels of METTL3/14. Rather, any impact on
387 VSV replication would likely be mediated by methylation of host factors. We perturbed the
388 expression of METTL3/14 using siRNAs or by overexpression and then determined the percent
389 of cells infected by VSV at 6 hours post-infection in the presence and absence of a low dose of
390 IFN-β pretreatment (6 hours; 25 U/mL). Measuring VSV infection at early time points after
391 infection allowed us to measure viral replication prior to cellular upregulation of ISGs induced
392 directly in response to infection. Indeed, in the absence of IFN-β pretreatment, we saw no
393 induction of ISGs by VSV in any condition (Figure 6A-B). Additionally, as anticipated, we found
394 that the replication of VSV, as measured by immunoblotting or quantifying the percent of cells
395 infected, was not altered by depletion or overexpression of METTL3/14 in cells in the absence of
396 IFN-β pretreatment (Figure 6). As observed earlier, following IFN-β pretreatment, METTL3/14
397 depletion led to decreased expression of METTL3/14-regulated ISGs (Figure 6A), while
398 METTL3/14 overexpression increased the expression of these ISGs (Figure 6B). As expected,
399 IFN-β pretreatment resulted in overall less replication of VSV, as IFN-β is known to inhibit VSV
400 replication (Muller et al., 1994) (Figure 6). However, upon depletion of METTL3/14, the ability of
401 IFN-β to restrict VSV was reduced (Figure 6A, 6C). Conversely, METTL3/14 overexpression
402 enhanced IFN-mediated restriction of VSV (Figure 6B, 6D). These data indicate that METTL3/14
403 enhances the antiviral properties of type I IFN and is required for an efficient IFN-mediated
404 antiviral response.

405

Figure 6



406

407

408 **Figure 6: METTL3/14 augments the antiviral effects of the type I IFN response. (A, B)**
 409 Representative immunoblot analysis (n=3) of extracts from Huh7 cells transfected with siRNAs
 410 (A) or stably overexpressing FLAG-METTL14, which also enhances METTL3 expression
 411 (M3/14^{OE}); (B), then treated with IFN- β (6 h) or mock, followed by infection with VSV (MOI=2; 6
 412 h). Arrows denote FLAG-METTL14 (top) and endogenous METLL14 (bottom). (C, D)
 413 Representative micrographs of Huh7 cells treated with non-targeting control (siCTRL) or
 414 METTL3/14 siRNA (C) or stably overexpressing FLAG-METTL14 (METTL3/14^{OE}; D), that were
 415 pre-treated with IFN- β (6 h), and then infected with VSV (MOI=2; 6 h), with quantification of
 416 percent of cells infected from 3 independent experiments with 5 fields per condition, with >150
 417 cells per field, normalized to siCTRL or WT with no IFN treatment, shown on the right. Scale Bar,
 418 100 μ m. Values are the mean \pm SEM of 3 biological replicates. * $p < 0.05$, *** $p < 0.001$ by 2-way
 419 ANOVA with Sidak's multiple comparisons test. ns = not significant.

420

421 Discussion

422 Post-transcriptional control of the type I IFN response remains poorly understood, and
 423 most of our existing knowledge centers around miRNA-mediated regulation of the IFN-induced
 424 JAK-STAT signaling pathway (Forster et al., 2015) or a few examples of alternative splicing of
 425 ISG transcripts (West et al., 2019). While a number of reports have documented non-canonical

426 activation or delayed stimulation of subsets of ISGs during viral infection, the molecular pathways
427 that can control these subsets of ISGs are not well understood (Pulit-Penalzo et al., 2012; Rose
428 et al., 2010). However, a number of studies have identified transcriptional regulators of subsets
429 of ISGs (Froggatt et al., 2019; Perwitasari et al., 2011; Seifert et al., 2019), and the mRNA Cap1
430 methyltransferase CMTR1 was recently shown to regulate the expression of certain ISGs
431 (Williams et al., 2020). These studies demonstrate the complexity of regulation of expression of
432 ISGs that extends beyond transcriptional induction of ISGs from signaling of the JAK-STAT
433 pathway. Here, we identify a novel post-transcriptional regulatory mechanism for the expression
434 of a subset of antiviral ISGs. We found that the m⁶A methyltransferase complex of METTL3/14
435 methylates certain antiviral ISGs to facilitate their translation to promote an antiviral cellular state.

436 The transcript-specific effects of m⁶A can modulate gene expression to coordinate cellular
437 responses. Indeed, we found that the presence of m⁶A on ISGs can elicit different mechanisms
438 of post-transcriptional regulation. For *IFITM1*, m⁶A in the 3' UTR led to an increase in its
439 translation, via METTL3/14 and the reader protein YTHDF1. Consistent with our results, previous
440 reports have shown that 3' UTR m⁶A modification enhances translation initiation and that YTHDF1
441 likely mediates this enhancement by recruiting eIF3 to m⁶A-modified mRNAs (Wang et al., 2015).
442 Interestingly, while the m⁶A-modified *MX1* is also upregulated at the protein level by METTL3/14,
443 YTHDF1 overexpression was not sufficient to elicit this upregulation. This may indicate that *MX1*
444 requires other factors or additional readers to enhance its expression. Indeed, YTHDF3 has
445 recently been shown to have roles in promoting translation of m⁶A-modified genes, perhaps by its
446 interaction with proteins of the 40S and 60S ribosomal subunits (Li et al., 2017; Shi et al., 2017),
447 and YTHDC2 can recognize m⁶A within coding sequence to enhance translation (Mao et al.,
448 2019). Of note, others have found that YTHDF3 inhibits ISG production in murine models through
449 its enhancement of *FOXO3* translation, although this apparently occurred independently of m⁶A
450 (Zhang et al., 2019b). Therefore, m⁶A and its related proteins can regulate ISG expression
451 through a variety of mechanisms. Indeed, only a subset of our identified m⁶A-modified ISGs were
452 translationally enhanced by METTL3/14, as shown by a combination of Ribo-seq, quantitative
453 mass spectrometry, and RNA-seq (Figure 5). As m⁶A has multiple functions in mRNA metabolism,
454 it is possible that m⁶A affects processes other than translation for these other modified ISGs, for
455 example by modulating their splicing, nuclear export, secondary structure, or stability (Liu et al.,
456 2019a). Indeed, it is likely that *ISG15* mRNA stability is regulated by m⁶A, as we found that this
457 transcript is bound by YTHDF1, appears to have an m⁶A site in its 3' UTR, and its mRNA levels
458 are increased following METTL3/14 depletion. m⁶A may also regulate mRNA trafficking or

459 turnover of ISGs at later timepoints after IFN stimulation or may contribute to alternative splicing
460 of antiviral genes in response to IFN.

461 Disentangling the regulatory effects of m⁶A on viral infection has been challenging, as both
462 viral and host transcripts contain m⁶A (Williams et al., 2019). Recent work by our group and others
463 revealed that m⁶A regulates several aspects of the host response to infection (Gokhale et al.,
464 2019; Rubio et al., 2018; Winkler et al., 2019). For example, when the *IFNB1* transcript is induced,
465 which can occur in response to viral infection, it is modified by m⁶A, and this destabilizes the
466 transcript. This regulation of *IFNB1* may serve as an intrinsic mechanism to dampen and control
467 the innate immune response (Rubio et al., 2018; Winkler et al., 2019). Interestingly, HCMV
468 appears to hijack this arm of immune regulation by upregulating METTL3/14 expression to
469 increase m⁶A on *IFNB1*, which ultimately decreases IFN- β production, resulting in enhanced viral
470 replication (Rubio et al., 2018; Winkler et al., 2019). However, in our work, by directly stimulating
471 ISGs with IFN- β , we reveal additional m⁶A-mediated regulation of certain ISGs downstream of
472 IFN- β production. Specifically, we show that METTL3/14 depletion reduces the ability of IFN to
473 restrict VSV infection, while METTL3/14 overexpression enhances the ability of IFN to inhibit VSV
474 infection (Figure 6). Importantly, as VSV replication was not affected by changes in METTL3/14
475 expression in the absence of IFN, this suggests that the differential ability of IFN to restrict VSV
476 following perturbation of METTL3/14 expression is not mediated by direct regulation of the viral
477 RNA (Figure 6). Rather, these data support the idea that METTL3/14 augments the antiviral
478 response by enhancing the production of ISGs. Identifying the factors that control m⁶A addition to
479 a specific subset of ISGs will be an important future pursuit and may clarify why only a subset of
480 these antiviral genes become methylated. Many type I IFN-stimulated genes are also induced by
481 type II (IFN- γ) and type III (IFN- λ) IFNs. Future studies may uncover whether signaling
482 downstream of these IFN families also leads to similar m⁶A-mediated modulation of ISG
483 expression. Additionally, exploring whether viruses employ strategies to counter METTL3/14-
484 mediated enhancement of ISGs will shed further light on the interplay between viral and host RNA
485 processes and how RNA modifications regulate these processes.

486 In addition to regulating type I IFN pathways, m⁶A tunes other cellular responses to viral
487 infection. We recently showed changes to the m⁶A status of certain host transcripts in response
488 to infection by *Flaviviridae*. Further, we found that many of these m⁶A-altered genes regulate
489 *Flaviviridae* infection (Gokhale et al., 2019). Some of the alterations in m⁶A during infection were
490 driven by innate immune sensing pathways, revealing that innate immune activation can affect
491 cellular m⁶A distribution during infection. Others have recently shown that VSV infection impairs
492 the demethylase activity of ALKBH5, resulting in increased m⁶A modification and destabilization

493 of the *OGDH* transcript. This resulted in less production of the metabolite itaconate, which
494 appeared to be required for VSV replication (Liu et al., 2019b). While these effects of m⁶A on VSV
495 replication occurred independently of IFN signaling, our work revealed that m⁶A can also inhibit
496 VSV replication by promoting ISG expression during IFN signaling. While we did not find an effect
497 of m⁶A on VSV replication in the absence of IFN signaling, as described above (Liu et al., 2019b),
498 we did not investigate a role for ALKBH5. Taken together, our findings add to the knowledge of
499 the diverse regulatory functions of m⁶A during host-pathogen interactions.

500 In summary, we reveal a subset of ISGs that are post-transcriptionally regulated by
501 METTL3/14 through m⁶A modification. Additionally, we show that the translation of these ISGs is
502 enhanced by m⁶A and postulate that m⁶A may be utilized during the IFN response as a strategy
503 for efficient production of antiviral proteins and the establishment of an antiviral cellular state.
504 Together, these data provide a new molecular understanding of type I IFN response regulation
505 that will ultimately broaden our understanding of innate immunity and host-pathogen interactions.
506 In addition to their functions in antiviral innate immunity, ISGs are also known to regulate
507 inflammation and cell death and recent reports have discovered roles for ISGs in cancer and
508 embryonic development (Buchrieser et al., 2019; Cheon et al., 2014; Yockey and Iwasaki, 2018).
509 Therefore, characterizing the molecular mechanisms that govern ISG expression will be essential
510 for understanding their dysregulation and this information could be harnessed to develop
511 therapeutics to alter ISG expression, which will be relevant to multiple diseases.

512

513 **Acknowledgements**

514 We thank colleagues who provided reagents (see Methods), New England Biolabs for the gift of
515 anti-m⁶A antibodies, the Duke Functional Genomics Core Facility, the Duke Center for Genomic
516 and Computational Biology Core, the Epigenomics Core and the Scientific Computing Unit at
517 Weill Cornell, and Horner lab members for manuscript discussion. This work was supported by
518 funds from Burroughs Wellcome Fund (S.M.H.) and National Institutes of Health: R01AI125416,
519 R21AI129851 (S.M.H. and C.E.M.), R01MH117406 (C.E.M.), T32-CA009111 (M.J.M.), R01-
520 GM127802 (B.X.). Other funding sources include: National Science and Engineering Research
521 Council of Canada (A.B.R.M. PGS-D funding), American Heart Association (N.S.G. Pre-doctoral
522 Fellowship, 17PRE33670017), National Institute of General Medical Sciences of the National
523 Institutes of Health Medical Scientist Training Program grant to the Weill
524 Cornell/Rockefeller/Sloan Kettering Tri-Institutional MD-PhD Program. (H.M. T32GM007739),
525 Bert L. and N. Kuggie Vallee Foundation, WorldQuant Foundation, Pershing Square Sohn
526 Cancer Research Alliance, NASA (NNX14AH50G).

527

528 **Author contributions**

529 Conceptualization: M.J.M. and S.M.H. Investigation: M.J.M., N.S.G., and H.I. Formal
530 analysis: M.J.M., A.B.R.M., H.M., N.S.A., and. Software: A.B.R.M., H.M., N.S.A. Writing – original
531 draft: M.J.M. and S.M.H. Writing – review and editing: M.J.M., A.B.R.M., H.M., N.S.A., N.S.G.,
532 B.X., C.E.M., and S.M.H. Funding acquisition: M.J.M., A.B.R.M., N.S.G., B.X., C.E.M., and S.M.H.

533

534 **Competing interests**

535 C.E.M. is a cofounder and board member for Biotia and Onegevity Health, and an advisor
536 or compensated speaker for Abbvie, Acuamark Diagnostics, ArcBio, Bio-Rad, DNA Genotek,
537 Genialis, Genpro, Illumina, New England Biolabs, QIAGEN, Whole Biome, and Zymo Research.

538

539 **Methods**

540 **Cell Lines.** Human hepatoma Huh7 cells, lung carcinoma A549 cells, neonatal human dermal
541 fibroblast (NHDF) cells, Vero cells, and embryonic kidney 293T cells were grown in Dulbecco's
542 modification of Eagle's medium (DMEM; Mediatech) supplemented with 10% fetal bovine serum
543 (Thermo Fisher Scientific), 1X minimum essential medium non-essential amino acids (Thermo
544 Fisher Scientific), and 25 mM HEPES (Thermo Fisher Scientific) (cDMEM). The identity of the
545 Huh7 cells used in this study was verified by using the GenePrint STR kit (Promega) (DNA
546 Analysis Facility, Duke University, Durham, NC, USA). A549 cells, 293T, and Vero cells (CCL-
547 185, CRL-3216, and CCL-81) were obtained from American Type Culture Collection (ATCC),
548 NHDF cells (CC-2509) were obtained from Lonza, and Huh7 cells were a gift of Dr. Michael Gale.
549 All cell lines were verified as mycoplasma free by the LookOut Mycoplasma PCR detection kit
550 (Sigma).

551

552 **IFN- β Treatment.** All IFN- β (PBL Assay Science) treatments were performed at a concentration
553 of 50 units/mL in cDMEM, unless otherwise noted.

554

555 **VSV Infection.** GFP-expressing VSV (Whelan et al., 2000) was obtained from Dr. Sean Whelan
556 and propagated by infecting Vero cells grown in cDMEM for 48 hours, after which infectious
557 supernatant was harvested and cleared by centrifugation (1,000 X g for 10 minutes at 4°C) and
558 frozen at -80°C prior to titering. To determine the titer of viral stocks, confluent Vero cells were
559 inoculated with serial dilutions of VSV in serum-free DMEM for 2 hours, overlaid with cDMEM
560 containing 2% SeaPlaque Agarose (Lonza), and incubated at 37°C for an additional 24 hours.

561 Cells were then fixed using 4% formaldehyde and visualized to count GFP-expressing plaques
562 and calculate plaque forming units/mL. Experimental VSV infections were performed at a
563 multiplicity of infection of 2 in serum-free DMEM for 1.5 h, after which cDMEM was replenished.
564 Cells were fixed in 4% formaldehyde, washed with PBS, and stained for DAPI (4',6-diamidino-2-
565 phenylindole) (Life Technologies, 1:1000). For each condition, 5 images were acquired at 10X
566 magnification on a Zeiss Axio Observer Z1 microscope, and images were processed using ZEN
567 2 (Zeiss). The percent of cells infected was calculated by counting the number of GFP-positive
568 cells / the number of nuclei (DAPI).

569
570 **Plasmids.** These plasmids have been described previously: pLEX-FLAG-YTHDF1 (Kennedy et
571 al., 2016), psiCheck2-m⁶A-null (Gokhale et al., 2019), psPAX2 (Addgene plasmid #12260;
572 RRID:Addgene_12260), and pMD2.G (Addgene plasmid # 12259; RRID:Addgene_12259). The
573 following plasmids were constructed in this study: pLEX-FLAG-METTL14, pLEX-FLAG-YTHDF1
574 W465A, and psiCheck2-m⁶A-null-ISRE-*IFITM1* 3' UTR reporter (wild-type and m⁶A-mut). pLEX-
575 FLAG-METTL14 was generated by cloning the PCR-amplified FLAG-tagged METTL14 coding
576 sequence into the BamHI and XhoI restriction sites of the pLEX expression vector. pLEX-FLAG-
577 YTHDF1 W465A was generated by site-directed mutagenesis of pLEX-FLAG-YTHDF1. WT and
578 m⁶A-mut *IFITM1* 3' UTR reporter plasmids (psiCheck2-m⁶A-null-ISRE-*IFITM1* 3' UTR reporter)
579 were generated by inserting either wild-type *IFITM1* 3' UTR cDNA or *IFITM1* 3' UTR cDNA with
580 4 A-to-G mutations at potential m⁶A sites (obtained as IDT gBlocks) into the XhoI and NotI
581 restriction sites of psiCheck2-m⁶A-null (Gokhale et al., 2019). The 5X ISRE promoter was PCR-
582 amplified from pISREluc (Sumpter et al., 2005) then inserted into the KpnI and NheI sites. All DNA
583 sequences were verified by sequencing.

584
585 **Transfection.** siRNAs directed against METTL3 (SI04317096), METTL14 (SI00459942), or non-
586 targeting AllStars negative control siRNA (1027280) were purchased from Qiagen. All siRNA
587 transfections were performed using the Lipofectamine RNAiMax reagent (Invitrogen), according
588 to manufacturer's instructions. siMETTL3/14 co-transfections were performed at a ratio of 1:2
589 siMETTL3:siMETTL14. Huh7 and A549 cells were transfected with 25 pmol of siRNA at a final
590 concentration of 0.0125 μ M, and NHDF cells were transfected with 250 pmol of siRNA at a final
591 concentration of 0.25 μ M. Media was changed 4 hours post-transfection, and cells were incubated
592 for 36 h post-transfection prior to each experimental treatment. Plasmid transfections of *IFITM1*
593 3' UTR reporter plasmids (500 ng per single well of a 6-well plate) were performed using the
594 FuGENE 6 (Promega), according to manufacturer's instructions.

595

596 **Generation of Overexpression Cell Lines.** Lentiviral particles were generated by harvesting
597 supernatant 72 h post-transfection of 293T cells with pLEX-FLAG-METTL14, pLEX-FLAG-
598 YTHDF1, or pLEX-FLAG-YTHDF1 W465A, and the packaging plasmids psPAX2 and pMD2.G
599 (provided by Duke Functional Genomics Facility). This supernatant was then used to transduce
600 Huh7 cells for 48 hours. Following transduction, cells were selected in 2 µg/mL puromycin (Sigma)
601 for 48 hours and then single cell colonies were isolated. Overexpression of FLAG-tagged proteins
602 in selected colonies was verified by immunoblotting, and we also verified that METTL14
603 overexpression stabilized METTL3 (Ping et al., 2014), creating METTL3/14 overexpression cell
604 lines. These clones were maintained in cDMEM containing 1 µg/mL puromycin.

605

606 **Immunoblotting.** Cells were lysed in a modified radioimmunoprecipitation assay (RIPA) buffer
607 (10 mM Tris [pH 7.5], 150 mM NaCl, 0.5% sodium deoxycholate, and 1% Triton X-100)
608 supplemented with protease inhibitor cocktail (Sigma) and phosphatase inhibitor cocktail II
609 (Millipore), and post-nuclear lysates were harvested by centrifugation. Quantified protein
610 (between 5 and 15 µg) was added to a 4X SDS protein sample buffer (40% glycerol, 240 mM
611 Tris-HCl [pH 6.8], 8% SDS, 0.04% bromophenol blue, 5% beta-mercaptoethanol), resolved by
612 SDS/PAGE, and transferred to nitrocellulose membranes in a 25 mM Tris-192 mM glycine-0.01%
613 SDS buffer. Membranes were stained with Revert 700 total protein stain (LI-COR Biosciences),
614 then blocked in 3% bovine serum albumin. Membranes were incubated with primary antibodies
615 for 2 hours at room temperature or overnight at 4°C. After washing with PBS-T buffer (1× PBS,
616 0.05% Tween 20), membranes were incubated with species-specific horseradish peroxidase-
617 conjugated antibodies (Jackson ImmunoResearch, 1:5000) for 1 hour at room temperature,
618 followed by treatment of the membrane with Clarity enhanced chemiluminescence (Bio-Rad) and
619 imaging on an Odyssey Fc imaging system (LI-COR Biosciences). The following antibodies were
620 used for immunoblotting: mouse anti-IFITM1 (Proteintech 60074-1-Ig, 1:1000; recognizes IFITM1
621 but not IFITM2 or IFITM3 (Shi et al., 2018; Xie et al., 2015)), rabbit anti-MX1 (Abcam ab207414,
622 1:1000), mouse anti-ISG15 (Santa Cruz sc-166755, 1:5000), rabbit anti-EIF2AK2 (Abcam
623 ab32506, 1:1000), rabbit anti-METTL14 (Sigma HPA038002, 1:2500), mouse anti-METTL3
624 (Abnova H00056339-B01P, 1:1000), rabbit anti-YTHDF1 (Proteintech 17479-1-AP, 1:1000),
625 mouse anti-FLAG-HRP (Sigma A8592, 1:5000), rabbit anti-GFP (Thermo Fisher Scientific A-
626 11122, 1:1000).

627

628 **Quantification of Immunoblots.** Following imaging using the LI-COR Odyssey Fc, immunoblots
629 were quantified using ImageStudio Lite software, and raw values were normalized to total protein
630 (Revert 700 total protein stain) for each condition.

631
632 **MeRIP-seq and Analysis.** Following mock or IFN- β treatment of Huh7 cells for 8 hours, cellular
633 RNA was harvested using TRIzol (Thermo Fisher Scientific), polyA-tailed mRNA was selected
634 using the Dynabeads mRNA Purification kit (Thermo Fisher Scientific), and MeRIP-seq was
635 performed using the NEB EpiMark m⁶A-enrichment kit as previously described (Gokhale et al.,
636 2019) with the following modifications. Briefly, 25 mL Protein G Dynabeads (Thermo Fisher) per
637 sample were washed three times in MeRIP buffer (150 mM NaCl, 10 mM Tris-HCl [pH 7.5], 0.1%
638 NP-40), and incubated with 1 mL anti-m⁶A antibody for 2 h at 4C with rotation. After washing
639 three times with MeRIP buffer, anti-m⁶A conjugated beads were incubated with purified mRNA
640 with rotation at 4C overnight in 300 mL MeRIP buffer with 1 mL RNase inhibitor (recombinant
641 RNasin; Promega). 10% of the mRNA sample was saved as the input fraction. Beads were then
642 washed twice with 500 mL MeRIP buffer, twice with low salt wash buffer (50 mM NaCl, 10 mM
643 Tris-HCl [pH 7.5], 0.1% NP-40), twice with high salt wash buffer (500 mM NaCl, 10 mM Tris-HCl
644 [pH 7.5], 0.1% NP-40), and once again with MeRIP buffer. m⁶A-modified RNA was eluted twice
645 in 100 mL of MeRIP buffer containing 5 mM m⁶A salt (Santa Cruz Biotechnology) for 30 min at
646 4C with rotation. Eluates were pooled and concentrated by ethanol purification. RNA-seq libraries
647 were prepared from both eluate and 10% input mRNA using the TruSeq mRNA library prep kit
648 (Illumina), subjected to quality control (MultiQC), and sequenced on the HiSeq 4000 instrument.
649 Reads were trimmed using Trimmomatic (Bolger et al., 2014) and aligned to the hg38 genome
650 using the splice-aware STAR aligner (Dobin et al., 2013). Changes in gene expression between
651 Mock and IFN- β treated samples were then identified using DESeq2 (Love et al., 2014) based on
652 differences in read counts from featureCounts (Liao et al., 2014) and plotted in Figure S2A. m⁶A
653 peaks were identified in IFN- β treated samples using the MeTDiff peak caller (Cui et al., 2018)
654 and additionally with meRIPPer (<https://sourceforge.net/projects/meripper/>). Presented data are
655 from MeTDiff analysis unless otherwise noted. Raw data from Winkler et al. (Winkler et al., 2019)
656 and Rubio et al. (Rubio et al., 2018) were similarly processed (Figure S2B). Coverage plots were
657 generated using CovFuzze (Imam et al., 2018) and a metagene plot for peak locations produced
658 as previously described (Gokhale et al., 2019). Motif enrichment was calculated using HOMER
659 (Heinz et al., 2010). Full methods and scripts for data processing are open-source and online on
660 GitHub (https://github.com/al-mcintyre/merip_reanalysis_scripts) (McIntyre et al., 2020).

661

662 **RT-qPCR.** Total cellular RNA was extracted using the Qiagen RNeasy kit (Life Technologies) or
663 TRIzol extraction (Thermo Fisher Scientific). RNA was then reverse transcribed using the iScript
664 cDNA synthesis kit (Bio-Rad) as per the manufacturer's instructions. The resulting cDNA was
665 diluted 1:5 in nuclease-free H₂O. RT-qPCR was performed in triplicate using the Power SYBR
666 Green PCR master mix (Thermo Fisher Scientific) and the Applied Biosystems Step One Plus or
667 QuantStudio 6 Flex RT-PCR systems. The oligonucleotide sequences used are listed in Table
668 S5.

669
670 **Nuclear/Cytoplasmic Fractionation.** Following siRNA treatment (36 h) and IFN- β treatment (20
671 h), cells were harvested and lysed in 200 μ L lysis buffer (10 mM Tris-HCl [pH 7.4], 140 mM NaCl,
672 1.5 mM MgCl₂, 10 mM EDTA, 0.5% Nonidet P-40 (NP-40)) on ice for 10 minutes. Following
673 centrifugation at 12000 X g at 4°C for 5 minutes, the supernatant (cytoplasmic fraction) was
674 collected, and the nuclear pellet was rinsed twice with lysis buffer. RNA was extracted from
675 cytoplasmic and nuclear pellets using TRIzol reagent and analyzed by RT-qPCR.

676
677 **Protein Stability Analysis.** Following siRNA treatment (36 h), Huh7 cells were treated with IFN-
678 β for 16 hours to induce ISGs. IFN- β was then replenished at half the dose in cDMEM containing
679 either DMSO as a control, or 50 μ g/mL cycloheximide (CHX, Sigma-Aldrich). Cells were harvested
680 over a timecourse (0, 2, 4, 6, 8, 12 hours post-CHX) and subjected to immunoblotting. Protein
681 stability was determined by measuring the protein remaining at each timepoint following CHX
682 treatment.

683
684 **Polysome Profiling.** Cells treated with siRNAs (36 h) were treated with IFN- β for 6 hours, then
685 pulsed with CHX (50 μ g/mL) for 10 minutes. Cells were harvested using trypsin and then lysed in
686 cytoplasmic lysis buffer (200 mM KCl, 25 mM HEPES [pH 7.0], 10 mM MgCl₂, 2% n-Dodecyl β -
687 D-maltoside (DDM; Chem-Impex), 0.2 mM CHX, 1 mM DTT, 40 U RNasin) for 15 minutes on ice.
688 Following clarification, lysates were ultracentrifuged on 15-50% sucrose gradients prepared in
689 polysome gradient buffer (200 mM KCl, 25 mM HEPES [pH 7.0], 15 mM MgCl₂, 1 mM DTT, 0.2
690 mM CHX) at 35,000 X g for 3.5 hours at 4°C. Following ultracentrifugation, 24 fractions were
691 collected from each sample using a BioComp Piston Gradient Fractionator instrument fitted with
692 a TRIAX flow cell to measure absorbance. RNA was extracted from each fraction using TRIzol
693 LS reagent (Thermo Fisher Scientific), and RNA quality was checked on a 1% agarose gel.
694 Following cDNA synthesis using the iScript cDNA synthesis kit (Bio-Rad), RT-qPCR was
695 performed using primers specific for each gene.

696

697 **MeRIP-RT-qPCR.** Total cellular RNA was harvested using TRIzol reagent and normalized to
698 equal input concentrations. m⁶A-positive and m⁶A-negative control oligonucleotides (EpiMark N6-
699 Methyladenosine Enrichment Kit, New England Biolabs) were spiked into total RNA prior to
700 immunoprecipitation. RNA was then immunoprecipitated with anti-m⁶A antibody (New England
701 Biolabs) overnight at 4°C with head-over-tail rotation, and then washed twice with 1X reaction
702 buffer (150mM NaCl, 10mM Tris-HCl, pH 7.5, 0.1% NP40), twice with low salt wash buffer (50
703 mM NaCl, 10 mM Tris-HCl, pH 7.5, 0.1% NP-40), twice with high salt wash buffer (500 mM NaCl,
704 10 mM Tris-HCl, pH 7.5, 0.1% NP-40), and once with 1X reaction buffer. RNA was eluted from
705 beads in elution buffer twice for 1 hour at 4°C, and then precipitated in isopropanol overnight at -
706 20°C, pelleted by centrifugation, and resuspended in nuclease-free water. Equal volumes of
707 eluted RNA and input RNA were used for cDNA synthesis and quantified by RT-qPCR. IP
708 efficiency was normalized by relative pulldown of spike-in positive controls.

709

710 **Luciferase Assays.** Following plasmid transfection of WT and m⁶A-mut IFITM1 3' UTR reporters
711 and mock or IFN-β treatment (12 h), a dual luciferase assay (Promega) was performed according
712 to manufacturer's instructions. Data was normalized as fold-change (IFN-β over mock) of the
713 value of *Renilla* luminescence divided by firefly luminescence, and values for WT IFITM1 3' UTR
714 reporter were set as 1.

715

716 **RNA Immunoprecipitation.** Following DNA transfection (16 h) and IFN-β treatment (8 h), cells
717 were harvested and lysed in polysome lysis buffer (100 mM KCl, 5 mM MgCl₂, 10 mM HEPES
718 [pH 7.0], 0.5% NP-40) supplemented with protease inhibitor cocktail (Sigma) and RNasin
719 ribonuclease inhibitor (Promega), and lysates were cleared by centrifugation. Ribonucleoprotein
720 complexes were immunoprecipitated with anti-FLAG M2 beads (Sigma) overnight at 4°C with
721 head-over-tail rotation, and then washed five times in ice-cold NT2 buffer (50 mM Tris-HCl [pH
722 7.4], 150 mM NaCl, 1 mM MgCl₂, 0.05% NP-40). Protein for immunoblotting was eluted from 25
723 percent of beads by boiling in 2X Laemmli sample buffer (Bio-Rad). RNA was extracted from 75
724 percent of beads using TRIzol reagent (Thermo Fisher Scientific). Equal volumes of eluted RNA
725 were used for cDNA synthesis, quantified by RT-qPCR, and normalized to RNA levels in input
726 samples. Enrichment over GFP was then calculated and plotted.

727

728 **RNA-seq.** Following siRNA treatment (36 h), Huh7 cells seeded in 10-cm² plates were stimulated
729 with IFN-β or mock treated (8 h), then harvested and RNA extraction was performed using TRIzol

730 reagent (Thermo Fisher Scientific). Samples were then treated with Turbo DNase I (Thermo
731 Fisher Scientific) according to manufacturer protocol and incubated at 37°C for 30 min, followed
732 by phenol/chloroform extraction and ethanol precipitation overnight. RNA concentrations were
733 then normalized. Sequencing libraries were prepared using the KAPA Stranded mRNA-Seq Kit
734 (Roche) and sequenced on an Illumina HiSeq 4000 with 100 bp paired-end reads by the Duke
735 University Center for Genomic and Computational Biology.

736

737 **Ribo-seq.** Following siRNA treatment (36 h), Huh7 cells seeded in 15-cm² plates were stimulated
738 with IFN- β (8 h), then washed with ice cold PBS, and flash frozen in liquid nitrogen. Cells were
739 then lysed in plates with polysome lysis buffer (20 mM Tris-HCl [pH 7.4], 150 mM NaCl, 5 mM
740 MgCl₂, 1 mM DTT, 1% Triton X-100, 25 U/mL Turbo DNase I (Thermo Fisher Scientific)), scraped,
741 and passed through a 25 gauge needle before collection in microfuge tubes and incubation for 15
742 minutes on ice. Cytoplasmic lysates were clarified by centrifugation. 5% of lysate was taken for
743 western blotting, and the remaining cytoplasmic lysate was supplemented with 0.4M CaCl₂ and
744 4000 gel units micrococcal nuclease (New England Biolabs), and incubated at 37°C (30 min) to
745 generate ribosome protected fragments (RPF RNA). RPF RNA was then ultracentrifuged (35000
746 X g at 4°C for 3.5 h), over 15-50% sucrose gradients in polysome gradient buffer (20 mM Tris-
747 HCl [pH 7.4], 150 mM NaCl, 5 mM MgCl₂, 1 mM DTT), after which 12 fractions were collected
748 from each sample using a BioComp Piston Gradient Fractionator instrument fitted with a TRIAX
749 flow cell to measure absorbance. Monosome fractions (fractions 6 and 7) were then pooled and
750 loaded onto a 100 kD molecular weight cut-off filter (Vivaspin 20) and centrifuged at 3000 X g at
751 4°C for 35 minutes to concentrate monosome-bound RPF RNA. The flow-through was discarded
752 and retained monosomes were separated from RPF RNA by adding polysome lysis buffer
753 supplemented with 50 mM EDTA and incubation on ice for 15 minutes. The resulting RPF RNA
754 solution was then re-applied to the emptied 100 kD molecular weight cut-off filter and centrifuged
755 at 3000 X g at 4°C for 15 minutes to separate RPF RNA from monosomes. The flow-through
756 containing the RPF RNA was then collected, phenol-chloroform extracted, and ethanol
757 precipitated. Precipitated RPF RNA samples were then run on a 15% TBE-Urea gel (Invitrogen),
758 and a band corresponding to 28-32 nucleotides was excised, crushed, and incubated in 0.4M
759 NaCl with 40 units of RNasin ribonuclease inhibitor (Promega) for 8 hours shaking at 4°C 1100
760 RPM. RNA was recovered by filtration through Corning Costar Spin-X columns (Sigma-Aldrich)
761 then isopropanol precipitated overnight. After resuspension, the remaining RNA was T4
762 Polynucleotide Kinase (New England Biolabs) treated, phenol-chloroform extracted, and
763 precipitated in ethanol overnight. Sequencing libraries for RPF samples were then generated

764 using the NEB Next small RNA library prep kit and these libraries were sequenced on an Illumina
765 NextSeq 500 High-output 75 bp with paired end reads by the Duke University Center for Genomic
766 and Computational Biology.

767

768 **RNA-seq and Ribo-seq Data Analysis.** Reads were evaluated using FastQC and trimmed using
769 cutadapt (Martin, 2011), followed by alignment to the hg38 human reference genome using the
770 STAR aligner with default parameters. The number of read fragments uniquely aligned to each
771 gene were counted with the Gencode v21 main comprehensive gene annotation file (aggregated
772 by gene_name) using featureCounts. Using a python script, the raw counts from each replicate
773 and condition were merged to generate a count matrix with N rows/genes and M samples/columns
774 (python scripts for count-matrix generation are open-source and online on GitHub
775 (https://github.com/hmourelatos/McFadden_ISG_m6a_countMatricies)). To identify differentially
776 expressed genes between various groups, we used DESeq2 (Love et al., 2014) to perform three
777 pairwise contrasts. First, with RNA-seq we compared the effects of IFN- β and mock treatment in
778 cells transfected with siCTRL (Table S1.1). Additional RNA-seq analyses included comparison of
779 siMETTL3/14 and siCTRL treated cells after both IFN- β and mock treatment (Tables S1.2 and
780 S1.3, respectively). Finally, with Ribo-seq, we compared siMETTL3/14 and siCTRL treated cells
781 following IFN- β treatment (Table S4). In each case, DESeq2 was applied with no additional
782 covariates and results shown in Tables S1.1, S1.2, and S3 respectively. Metagene plots from
783 Ribo-seq reads were composed using deepTools v3.1 (Ramírez et al., 2016) with the
784 computeMatrix utility. RNA-seq heatmap was generated using R software, and the heatmap for
785 Ribo-seq was generated using ClustVis (Metsalu and Vilo, 2015).

786

787 **Mass Spectrometry.** Prior to the siRNA experiments, cells were grown for at least 12 generations
788 in DMEM medium without Lysine and Arginine (#PI88420), supplemented with Dialyzed FBS
789 (#26000044), either light or heavy L-Arginine and L-Lysine (L-Arginine-HCl #PI88427; L-Arginine-
790 HCl, 13C6, 15N4 #PI88434; L-Lysine-2HCl #PI88429; L-Lysine-2HCl, 13C6, 15N2 #PI88432),
791 and 100 U/ml penicillin, 100 μ g/ml streptomycin and 2 mM L-glutamine. Following stable isotope
792 labeling, siRNA-treated cells (36 h) were stimulated with IFN- β for 24 hours prior to harvest by
793 trypsinization and lysis in RIPA buffer supplemented with protease inhibitor cocktail (Sigma) and
794 phosphatase inhibitor cocktail II (Millipore), and post-nuclear lysates were harvested by
795 centrifugation. 5 μ L at 1 μ g/ μ L of siMETTL3/14 (Heavy) extracts were mixed with 5 μ L at 1 μ g/ μ L
796 of siCTRL (Light) extracts for the Forward experiment, and 5 μ L at 1 μ g/ μ L of siMETTL3/14 (Light)
797 extracts were mixed with 5 μ L at 1 μ g/ μ L of siCTRL (Heavy) extracts for the Reverse experiment.

798 The lysates were run on a 4-12% Bis-Tris gel for 30 min. The gel was stained with Colloidal
799 Coomassie and a single patch was cut and processed for each sample. The gel patches were
800 digested with trypsin. The resulting peptides were cleaned with a C18 tip. Liquid chromatography
801 was performed with an EASY-nLC™ 1000 Integrated Ultra High Pressure Nano-HPLC System
802 and MS/MS with a Q-EXACTIVE System equipped with a Nanospray Flex Ion Source, as
803 previously described (Abell et al., 2017).

804

805 **Mass Spectrometry data analysis.** Four RAW files representing two replicates each of Forward
806 and Reverse SILAC experiments were retrieved from the Orbitrap. Heavy/light label ratios were
807 quantified across all samples using MaxQuant v1.6.7.0 with the Andromeda search engine and
808 default parameters other than specifying SILAC labels (Cox and Mann, 2008; Cox et al., 2011).
809 For all analyses, the “H/L Ratio – Normalized” field containing median-centered label ratios was
810 extracted for each peptide and/or protein and compared across replicates (Table S3). Heatmaps
811 for mass spectrometry were generated using ClustVis (Metsalu and Vilo, 2015).

812

813 Peptide regression modeling:

814 To take advantage of the measurement independence of unique peptides, we applied a simple
815 linear mixed model to identify significant shifts in labeling ratio between conditions while
816 accounting for peptide-specific effects. First, we merge all proteins that are described by the same
817 set of peptide ratios (e.g. protein sequences from the same gene for which all detected peptides
818 are shared). Then, for each protein (defined now as a set of peptide ratios), we fit a linear model
819 of the following form using lme4 in R (Bates et al., 2015)

820

$$r \sim Z\mathbf{u}_{pep} + X\beta_{label} + \epsilon$$

821 where:

- 822 • r is the median-normalized heavy/light label ratio derived from MaxQuant
- 823 • Z is a binary design matrix indicating the peptide identity of each ratio measurement
- 824 • X is a binary design vector indicating condition (forward or reverse)
- 825 • \mathbf{u}_{pep} is a vector of random effects corresponding to each peptide effect
- 826 • β_{label} is the fixed effect of condition

827 Thus, each peptide ratio is described as the sum of a peptide-level random effect and a condition
828 (forward vs reverse) fixed effect, and some error. We extract effect size estimates and p-values
829 from unmodified Wald tests on the fixed effect of condition, and adjust across all proteins with the
830 Benjamini-Hochberg (BH) procedure. Note that in the less-powerful case of proteins with only one

831 measured peptide, the random peptide effect is just a constant and the model reduces to simply
832 comparing the means of the forward and reverse replicate ratios for the single peptide.

833

834 Aggregating proteins for gene-level results:

835 Peptide regression modeling generates one test for each protein, so many genes are tested
836 multiple times at each of their proteins. Annotated reference protein sequences often contain
837 multiple entries per gene with varying degrees of similarity. After applying the procedure above,
838 we observe as expected that the vast majority of genes contain either all significant or all non-
839 significant protein results. We conservatively describe as significant any gene with a significant
840 maximum p-value (meaning all tested proteins are significant) following multiple test correction.

841

842 **Lead Contact and Materials Availability.** Further information and requests for resources and
843 reagents should be directed to and will be fulfilled by the Lead Contact, Stacy M. Horner
844 (stacy.horner@duke.edu).

845

846 **Data Availability.** All raw data from RNA-seq, MeRIP-seq, and Ribo-seq are available through
847 GEO (accession number: GSE155448).

848 Raw data from mass spectrometry are available at the following URLs:

849 <https://web.corral.tacc.utexas.edu/xhemalce/Forward1.raw>

850 <https://web.corral.tacc.utexas.edu/xhemalce/Forward2.raw>

851 <https://web.corral.tacc.utexas.edu/xhemalce/Reverse1.raw>

852 <https://web.corral.tacc.utexas.edu/xhemalce/Reverse2.raw>

853

854 **Supplemental Information**

855 Supplemental information Figures S1-S4.

856 Table S1: RNA-seq analysis of gene expression changes following IFN- β treatment and
857 METTL3/14 depletion.

- 858 • Table S1.1: siCTRL IFN / siCTRL Mock
- 859 • Table S1.2: siMETTL3/14 Mock / siCTRL Mock
- 860 • Table S1.3: siMETTL3/14 IFN / siCTRL IFN

861 Table S2: m⁶A peaks in the IFN- β induced transcriptome.

- 862 • Table S2.1: Input RNA-seq Analysis (IFN / Mock)
- 863 • Table S2.2: MeTDiff m⁶A Peaks
- 864 • Table S2.3: meRIPPer m⁶A Peaks

865 Table S3: Analysis of METTL3/14 depletion effect on protein expression using quantitative mass
866 spectrometry.

867 Table S4: Analysis of Ribo-seq data from METTL3/14 depletion and IFN- β treatment.

868 Table S5: List of oligonucleotides and siRNAs used in this study.

869

870

871 **References**

872

873 Abell, N.S., Mercado, M., Caneque, T., Rodriguez, R., and Xhemalce, B. (2017). Click
874 Quantitative Mass Spectrometry Identifies PIWIL3 as a Mechanistic Target of RNA Interference
875 Activator Enoxacin in Cancer Cells. *J. Am. Chem. Soc.* *139*, 1400-1403.

876 Banchereau, J., and Pascual, V. (2006). Type I interferon in systemic lupus erythematosus and
877 other autoimmune diseases. *Immunity* *25*, 383-392.

878 Bates, D., Mächler, M., Bolker, B., and Walker, S. (2015). Fitting Linear Mixed-Effects Models
879 Using lme4. *Journal of Statistical Software* *67*, 48.

880 Bolger, A.M., Lohse, M., and Usadel, B. (2014). Trimmomatic: a flexible trimmer for Illumina
881 sequence data. *Bioinformatics* *30*, 2114-2120.

882 Boulias, K., Toczydlowska-Socha, D., Hawley, B.R., Liberman, N., Takashima, K., Zaccara, S.,
883 Guez, T., Vasseur, J.J., Debart, F., Aravind, L., *et al.* (2019). Identification of the m(6)Am
884 Methyltransferase PCIF1 Reveals the Location and Functions of m(6)Am in the Transcriptome.
885 *Mol. Cell* *75*, 631-643.e638.

886 Buchrieser, J., Degrelle, S.A., Couderc, T., Nevers, Q., Disson, O., Manet, C., Donahue, D.A.,
887 Porrot, F., Hillion, K.H., Perthame, E., *et al.* (2019). IFITM proteins inhibit placental
888 syncytiotrophoblast formation and promote fetal demise. *Science* *365*, 176-180.

889 Chen, Y.G., Chen, R., Ahmad, S., Verma, R., Kasturi, S.P., Amaya, L., Broughton, J.P., Kim, J.,
890 Cadena, C., Pulendran, B., *et al.* (2019). N6-Methyladenosine Modification Controls Circular
891 RNA Immunity. *Mol. Cell* *76*, 96-109.e109.

892 Cheon, H., Borden, E.C., and Stark, G.R. (2014). Interferons and their stimulated genes in the
893 tumor microenvironment. *Semin. Oncol.* *41*, 156-173.

894 Coats, R.A., Liu, X.M., Mao, Y., Dong, L., Zhou, J., Wan, J., Zhang, X., and Qian, S.B. (2017).
895 m(6)A Facilitates eIF4F-Independent mRNA Translation. *Mol. Cell* *68*, 504-514.e507.

896 Cox, J., and Mann, M. (2008). MaxQuant enables high peptide identification rates, individualized
897 p.p.b.-range mass accuracies and proteome-wide protein quantification. *Nat. Biotechnol.* *26*,
898 1367-1372.

899 Cox, J., Neuhauser, N., Michalski, A., Scheltema, R.A., Olsen, J.V., and Mann, M. (2011).
900 Andromeda: a peptide search engine integrated into the MaxQuant environment. *J. Proteome*
901 *Res.* *10*, 1794-1805.

- 902 Cui, X., Zhang, L., Meng, J., Rao, M.K., Chen, Y., and Huang, Y. (2018). MeTDiff: A Novel
903 Differential RNA Methylation Analysis for MeRIP-Seq Data. *IEEE/ACM Trans. Comput. Biol.*
904 *Bioinform.* 15, 526-534.
- 905 Dobin, A., Davis, C.A., Schlesinger, F., Drenkow, J., Zaleski, C., Jha, S., Batut, P., Chaisson,
906 M., and Gingeras, T.R. (2013). STAR: ultrafast universal RNA-seq aligner. *Bioinformatics* 29,
907 15-21.
- 908 Dominissini, D., Moshitch-Moshkovitz, S., Schwartz, S., Salmon-Divon, M., Ungar, L.,
909 Osenberg, S., Cesarkas, K., Jacob-Hirsch, J., Amariglio, N., Kupiec, M., *et al.* (2012). Topology
910 of the human and mouse m6A RNA methylomes revealed by m6A-seq. *Nature* 485, 201-206.
- 911 Durbin, A.F., Wang, C., Marcotrigiano, J., and Gehrke, L. (2016). RNAs Containing Modified
912 Nucleotides Fail To Trigger RIG-I Conformational Changes for Innate Immune Signaling. *mBio*
913 7.
- 914 Fang, T.C., Schaefer, U., Mecklenbrauker, I., Stienen, A., Dewell, S., Chen, M.S., Rioja, I.,
915 Parravicini, V., Prinjha, R.K., Chandwani, R., *et al.* (2012). Histone H3 lysine 9 di-methylation as
916 an epigenetic signature of the interferon response. *J. Exp. Med.* 209, 661-669.
- 917 Feng, Z., Li, Q., Meng, R., Yi, B., and Xu, Q. (2018). METTL3 regulates alternative splicing of
918 MyD88 upon the lipopolysaccharide-induced inflammatory response in human dental pulp cells.
919 *J. Cell. Mol. Med.* 22, 2558-2568.
- 920 Forster, S.C., Tate, M.D., and Hertzog, P.J. (2015). MicroRNA as Type I Interferon-Regulated
921 Transcripts and Modulators of the Innate Immune Response. *Front. Immunol.* 6, 334.
- 922 Froggatt, H.M., Harding, A.T., and Heaton, N.S. (2019). ETV7 represses a subset of interferon-
923 stimulated genes that restrict influenza viruses. *bioRxiv*, 851543.
- 924 Gokhale, N.S., McIntyre, A.B.R., Mattocks, M.D., Holley, C.L., Lazear, H.M., Mason, C.E., and
925 Horner, S.M. (2019). Altered m(6)A Modification of Specific Cellular Transcripts Affects
926 Flaviviridae Infection. *Mol. Cell.*
- 927 Gonzalez-Navajas, J.M., Lee, J., David, M., and Raz, E. (2012). Immunomodulatory functions of
928 type I interferons. *Nat. Rev. Immunol.* 12, 125-135.
- 929 Heinz, S., Benner, C., Spann, N., Bertolino, E., Lin, Y.C., Laslo, P., Cheng, J.X., Murre, C.,
930 Singh, H., and Glass, C.K. (2010). Simple combinations of lineage-determining transcription
931 factors prime cis-regulatory elements required for macrophage and B cell identities. *Mol. Cell*
932 38, 576-589.
- 933 Huang, M., Qian, F., Hu, Y., Ang, C., Li, Z., and Wen, Z. (2002). Chromatin-remodelling factor
934 BRG1 selectively activates a subset of interferon-alpha-inducible genes. *Nat. Cell Biol.* 4, 774-
935 781.

- 936 Imam, H., Khan, M., Gokhale, N.S., McIntyre, A.B.R., Kim, G.W., Jang, J.Y., Kim, S.J., Mason,
937 C.E., Horner, S.M., and Siddiqui, A. (2018). N6-methyladenosine modification of hepatitis B
938 virus RNA differentially regulates the viral life cycle. *Proc. Natl. Acad. Sci. U. S. A.* *115*, 8829-
939 8834.
- 940 Kariko, K., Buckstein, M., Ni, H., and Weissman, D. (2005). Suppression of RNA recognition by
941 Toll-like receptors: the impact of nucleoside modification and the evolutionary origin of RNA.
942 *Immunity* *23*, 165-175.
- 943 Kennedy, E.M., Bogerd, H.P., Kornepati, A.V., Kang, D., Ghoshal, D., Marshall, J.B., Poling,
944 B.C., Tsai, K., Gokhale, N.S., Horner, S.M., *et al.* (2016). Posttranscriptional m(6)A Editing of
945 HIV-1 mRNAs Enhances Viral Gene Expression. *Cell Host Microbe* *19*, 675-685.
- 946 Lesbirel, S., and Wilson, S.A. (2019). The m(6)Amethylase complex and mRNA export. *Biochim*
947 *Biophys Acta Gene Regul Mech* *1862*, 319-328.
- 948 Li, A., Chen, Y.S., Ping, X.L., Yang, X., Xiao, W., Yang, Y., Sun, H.Y., Zhu, Q., Baidya, P.,
949 Wang, X., *et al.* (2017). Cytoplasmic m(6)A reader YTHDF3 promotes mRNA translation. *Cell*
950 *Res.* *27*, 444-447.
- 951 Liao, Y., Smyth, G.K., and Shi, W. (2014). featureCounts: an efficient general purpose program
952 for assigning sequence reads to genomic features. *Bioinformatics* *30*, 923-930.
- 953 Lin, S., Choe, J., Du, P., Triboulet, R., and Gregory, R.I. (2016). The m(6)A Methyltransferase
954 METTL3 Promotes Translation in Human Cancer Cells. *Mol. Cell* *62*, 335-345.
- 955 Liu, H., Kang, H., Liu, R., Chen, X., and Zhao, K. (2002). Maximal induction of a subset of
956 interferon target genes requires the chromatin-remodeling activity of the BAF complex. *Mol.*
957 *Cell. Biol.* *22*, 6471-6479.
- 958 Liu, J., Harada, B.T., and He, C. (2019a). Regulation of Gene Expression by N(6)-
959 methyladenosine in Cancer. *Trends Cell Biol.* *29*, 487-499.
- 960 Liu, J., Yue, Y., Han, D., Wang, X., Fu, Y., Zhang, L., Jia, G., Yu, M., Lu, Z., Deng, X., *et al.*
961 (2014). A METTL3-METTL14 complex mediates mammalian nuclear RNA N6-adenosine
962 methylation. *Nat. Chem. Biol.* *10*, 93-95.
- 963 Liu, Y., You, Y., Lu, Z., Yang, J., Li, P., Liu, L., Xu, H., Niu, Y., and Cao, X. (2019b). N (6)-
964 methyladenosine RNA modification-mediated cellular metabolism rewiring inhibits viral
965 replication. *Science* *365*, 1171-1176.
- 966 Love, M.I., Huber, W., and Anders, S. (2014). Moderated estimation of fold change and
967 dispersion for RNA-seq data with DESeq2. *Genome Biol.* *15*, 550.

- 968 Lu, M., Zhang, Z., Xue, M., Zhao, B.S., Harder, O., Li, A., Liang, X., Gao, T.Z., Xu, Y., Zhou, J.,
969 *et al.* (2020). N(6)-methyladenosine modification enables viral RNA to escape recognition by
970 RNA sensor RIG-I. *Nat Microbiol* 5, 584-598.
- 971 Mao, Y., Dong, L., Liu, X.M., Guo, J., Ma, H., Shen, B., and Qian, S.B. (2019). m(6)A in mRNA
972 coding regions promotes translation via the RNA helicase-containing YTHDC2. *Nat Commun*
973 10, 5332.
- 974 Martin, M. (2011). Cutadapt removes adapter sequences from high-throughput sequencing
975 reads. *EMBnet Journal* 17, 10-12.
- 976 McIntyre, A.B.R., Gokhale, N.S., Cerchiatti, L., Jaffrey, S.R., Horner, S.M., and Mason, C.E.
977 (2020). Limits in the detection of m(6)A changes using MeRIP/m(6)A-seq. *Sci. Rep.* 10, 6590.
- 978 Metsalu, T., and Vilo, J. (2015). ClustVis: a web tool for visualizing clustering of multivariate
979 data using Principal Component Analysis and heatmap. *Nucleic Acids Res.* 43, W566-570.
- 980 Meyer, K.D., and Jaffrey, S.R. (2017). Rethinking m(6)A Readers, Writers, and Erasers. *Annu.*
981 *Rev. Cell Dev. Biol.* 33, 319-342.
- 982 Meyer, K.D., Saletore, Y., Zumbo, P., Elemento, O., Mason, C.E., and Jaffrey, S.R. (2012).
983 Comprehensive analysis of mRNA methylation reveals enrichment in 3' UTRs and near stop
984 codons. *Cell* 149, 1635-1646.
- 985 Miller, D.M., Zhang, Y., Rahill, B.M., Waldman, W.J., and Sedmak, D.D. (1999). Human
986 cytomegalovirus inhibits IFN-alpha-stimulated antiviral and immunoregulatory responses by
987 blocking multiple levels of IFN-alpha signal transduction. *J. Immunol.* 162, 6107-6113.
- 988 Muller, U., Steinhoff, U., Reis, L.F., Hemmi, S., Pavlovic, J., Zinkernagel, R.M., and Aguet, M.
989 (1994). Functional role of type I and type II interferons in antiviral defense. *Science* 264, 1918-
990 1921.
- 991 Ogino, T., and Banerjee, A.K. (2011). An unconventional pathway of mRNA cap formation by
992 vesiculoviruses. *Virus Res.* 162, 100-109.
- 993 Perwitasari, O., Cho, H., Diamond, M.S., and Gale, M., Jr. (2011). Inhibitor of κ B kinase epsilon
994 (IKK(epsilon)), STAT1, and IFIT2 proteins define novel innate immune effector pathway against
995 West Nile virus infection. *J. Biol. Chem.* 286, 44412-44423.
- 996 Ping, X.L., Sun, B.F., Wang, L., Xiao, W., Yang, X., Wang, W.J., Adhikari, S., Shi, Y., Lv, Y.,
997 Chen, Y.S., *et al.* (2014). Mammalian WTAP is a regulatory subunit of the RNA N6-
998 methyladenosine methyltransferase. *Cell Res.* 24, 177-189.
- 999 Pulit-Penalzoza, J.A., Scherbik, S.V., and Brinton, M.A. (2012). Type 1 IFN-independent
1000 activation of a subset of interferon stimulated genes in West Nile virus Eg101-infected mouse
1001 cells. *Virology* 425, 82-94.

- 1002 Ramírez, F., Ryan, D.P., Grüning, B., Bhardwaj, V., Kilpert, F., Richter, A.S., Heyne, S., Dündar,
1003 F., and Manke, T. (2016). deepTools2: a next generation web server for deep-sequencing data
1004 analysis. *Nucleic Acids Res.* *44*, W160-165.
- 1005 Rose, K.M., Elliott, R., Martinez-Sobrido, L., Garcia-Sastre, A., and Weiss, S.R. (2010). Murine
1006 coronavirus delays expression of a subset of interferon-stimulated genes. *J. Virol.* *84*, 5656-
1007 5669.
- 1008 Rubio, R.M., Depledge, D.P., Bianco, C., Thompson, L., and Mohr, I. (2018). RNA m(6) A
1009 modification enzymes shape innate responses to DNA by regulating interferon beta. *Genes*
1010 *Dev.* *32*, 1472-1484.
- 1011 Schoggins, J.W. (2014). Interferon-stimulated genes: roles in viral pathogenesis. *Curr. Opin.*
1012 *Virol.* *6*, 40-46.
- 1013 Schoggins, J.W. (2019). Interferon-Stimulated Genes: What Do They All Do? Annual review of
1014 virology *6*, 567-584.
- 1015 Schoggins, J.W., and Rice, C.M. (2011). Interferon-stimulated genes and their antiviral effector
1016 functions. *Curr. Opin. Virol.* *1*, 519-525.
- 1017 Seifert, L.L., Si, C., Saha, D., Sadic, M., de Vries, M., Ballentine, S., Briley, A., Wang, G.,
1018 Valero-Jimenez, A.M., Mohamed, A., *et al.* (2019). The ETS transcription factor ELF1 regulates
1019 a broadly antiviral program distinct from the type I interferon response. *PLoS Pathog.* *15*,
1020 e1007634.
- 1021 Sendinc, E., Valle-Garcia, D., Dhall, A., Chen, H., Henriques, T., Navarrete-Perea, J., Sheng,
1022 W., Gygi, S.P., Adelman, K., and Shi, Y. (2019). PCIF1 Catalyzes m6Am mRNA Methylation to
1023 Regulate Gene Expression. *Mol. Cell* *75*, 620-630.e629.
- 1024 Shaw, A.E., Hughes, J., Gu, Q., Behdenna, A., Singer, J.B., Dennis, T., Orton, R.J., Varela, M.,
1025 Gifford, R.J., Wilson, S.J., *et al.* (2017). Fundamental properties of the mammalian innate
1026 immune system revealed by multispecies comparison of type I interferon responses. *PLoS Biol.*
1027 *15*, e2004086.
- 1028 Shi, G., Ozog, S., Torbett, B.E., and Compton, A.A. (2018). mTOR inhibitors lower an intrinsic
1029 barrier to virus infection mediated by IFITM3. *Proc. Natl. Acad. Sci. U. S. A.* *115*, E10069-
1030 e10078.
- 1031 Shi, H., Wang, X., Lu, Z., Zhao, B.S., Ma, H., Hsu, P.J., Liu, C., and He, C. (2017). YTHDF3
1032 facilitates translation and decay of N(6)-methyladenosine-modified RNA. *Cell Res.* *27*, 315-328.
- 1033 Shi, H., Wei, J., and He, C. (2019). Where, When, and How: Context-Dependent Functions of
1034 RNA Methylation Writers, Readers, and Erasers. *Mol. Cell* *74*, 640-650.

- 1035 Stark, G.R., and Darnell, J.E., Jr. (2012). The JAK-STAT pathway at twenty. *Immunity* 36, 503-
1036 514.
- 1037 Sumpter, R., Jr., Loo, Y.M., Foy, E., Li, K., Yoneyama, M., Fujita, T., Lemon, S.M., and Gale,
1038 M., Jr. (2005). Regulating intracellular antiviral defense and permissiveness to hepatitis C virus
1039 RNA replication through a cellular RNA helicase, RIG-I. *J. Virol.* 79, 2689-2699.
- 1040 Teijaro, J.R. (2016). Type I interferons in viral control and immune regulation. *Curr. Opin. Virol.*
1041 16, 31-40.
- 1042 Wang, X., Lu, Z., Gomez, A., Hon, G.C., Yue, Y., Han, D., Fu, Y., Parisien, M., Dai, Q., Jia, G.,
1043 *et al.* (2014). N6-methyladenosine-dependent regulation of messenger RNA stability. *Nature*
1044 505, 117-120.
- 1045 Wang, X., Zhao, B.S., Roundtree, I.A., Lu, Z., Han, D., Ma, H., Weng, X., Chen, K., Shi, H., and
1046 He, C. (2015). N(6)-methyladenosine Modulates Messenger RNA Translation Efficiency. *Cell*
1047 161, 1388-1399.
- 1048 West, K.O., Scott, H.M., Torres-Odio, S., West, A.P., Patrick, K.L., and Watson, R.O. (2019).
1049 The Splicing Factor hnRNP M Is a Critical Regulator of Innate Immune Gene Expression in
1050 Macrophages. *Cell reports* 29, 1594-1609.e1595.
- 1051 Whelan, S.P., Barr, J.N., and Wertz, G.W. (2000). Identification of a minimal size requirement
1052 for termination of vesicular stomatitis virus mRNA: implications for the mechanism of
1053 transcription. *J. Virol.* 74, 8268-8276.
- 1054 Williams, G.D., Gokhale, N.S., and Horner, S.M. (2019). Regulation of Viral Infection by the
1055 RNA Modification N6-Methyladenosine. *Annu Rev Virol* 6, 235-253.
- 1056 Williams, G.D., Gokhale, N.S., Snider, D.L., and Horner, S.M. (2020). The mRNA Cap 2'-O-
1057 Methyltransferase CMTR1 Regulates the Expression of Certain Interferon-Stimulated Genes.
1058 *mSphere* 5.
- 1059 Winkler, R., Gillis, E., Lasman, L., Safra, M., Geula, S., Soyris, C., Nachshon, A., Tai-
1060 Schmiedel, J., Friedman, N., Le-Trilling, V.T.K., *et al.* (2019). m(6)A modification controls the
1061 innate immune response to infection by targeting type I interferons. *Nat. Immunol.* 20, 173-182.
- 1062 Xie, M., Xuan, B., Shan, J., Pan, D., Sun, Y., Shan, Z., Zhang, J., Yu, D., Li, B., and Qian, Z.
1063 (2015). Human cytomegalovirus exploits interferon-induced transmembrane proteins to facilitate
1064 morphogenesis of the virion assembly compartment. *J. Virol.* 89, 3049-3061.
- 1065 Xu, C., Liu, K., Ahmed, H., Loppnau, P., Schapira, M., and Min, J. (2015). Structural Basis for
1066 the Discriminative Recognition of N6-Methyladenosine RNA by the Human YT521-B Homology
1067 Domain Family of Proteins. *J. Biol. Chem.* 290, 24902-24913.

- 1068 Yockey, L.J., and Iwasaki, A. (2018). Interferons and Proinflammatory Cytokines in Pregnancy
1069 and Fetal Development. *Immunity* *49*, 397-412.
- 1070 Zaccara, S., and Jaffrey, S.R. (2020). A Unified Model for the Function of YTHDF Proteins in
1071 Regulating m(6)A-Modified mRNA. *Cell* *181*, 1582-1595.e1518.
- 1072 Zhang, C., Fu, J., and Zhou, Y. (2019a). A Review in Research Progress Concerning m6A
1073 Methylation and Immunoregulation. *Front. Immunol.* *10*, 922.
- 1074 Zhang, Y., Wang, X., Zhang, X., Wang, J., Ma, Y., Zhang, L., and Cao, X. (2019b). RNA-binding
1075 protein YTHDF3 suppresses interferon-dependent antiviral responses by promoting FOXO3
1076 translation. *Proc. Natl. Acad. Sci. U. S. A.* *116*, 976-981.
- 1077 Zheng, Q., Hou, J., Zhou, Y., Li, Z., and Cao, X. (2017). The RNA helicase DDX46 inhibits
1078 innate immunity by entrapping m(6)A-demethylated antiviral transcripts in the nucleus. *Nat.*
1079 *Immunol.* *18*, 1094-1103.
- 1080
- 1081